Supplementary Information: Gibbs-Duhem-Informed Neural Networks for Binary Activity Coefficient Prediction

Jan G. Rittig,[a] Kobi C. Felton,[b] Alexei A. Lapkin[b], and Alexander Mitsos[*,c,a,d]

[a]Process Systems Engineering (AVT.SVT), RWTH Aachen University, Forckenbeckstraße 51, 52074 Aachen, Germany.

[b]Department of Chemical Engineering and Biotechnology, University of Cambridge Philippa Fawcett Dr, Cambridge CB3 0AS, UK.

[c]JARA-ENERGY, 52056 Aachen, Templergraben 55, Germany.

[d]Institute of Energy and Climate Research: Energy Systems Engineering (IEK-10), Forschungszentrum Jülich GmbH, Wilhelm-Johnen-Straße, 52425 Jülich, Germany.

September 5, 2023

1 Effect of MLP structure on thermodynamic consistency

During the development of the MCM structure, we noticed different behavior in the prediction quality and thermodynamic consistency of the models related to the final prediction MLP structure. Specifically, we investigated MCM models with different MLP heads: multi-MLP, i.e., two independent MLPs predicting $\ln(\gamma_1)$ and $\ln(\gamma_2)$, respectively; multi-MLP with 1 shared layer; multi-MLP with 2 shared layers; and a single-MLP having shared layers only and two output neurons for the respective $\ln(\gamma_i)$ predictions. Note that all models are trained with standard prediction loss, thus without Gibbs-Duhem loss, and with ReLU as activation function.

Figure S1 presents the performance on activity coefficient predictions (S1a) and thermodynamic consistency (S1b) in histograms for the different architectures. We further show the composition-dependent errors in Figures S1c, S1d. The overall prediction accuracy and thermodynamic consistency are very similar for all architectures. For the composition-dependent prediction accuracies, we also observe similar values except for $x_i = 1$, where the more intertwined MLPs, i.e., multi-MLP with 2 shared layers and the single-MLP show larger errors. Interestingly, the composition-dependent thermodynamic consistencies show opposing behaviour for the different models. That is, the mutli-MLP shows the lowest errors at boundary compositions ($x_i = 0$ and $x_i = 1$), whereas the single-MLP performs best at intermediate compositions. The more separated multi-MLP with 1 shared layer shows similar behaviour to the multi-MLP, and the more intertwined multi-MLP with 2 shared layers matches the single-MLP behaviour.

Given these observations, we also implemented a version of the GNN with a single MLP and multi MLPs with shared layers operating on the concatenated embeddings of the solvents. Please note that these GNN adaptions do not preserve the input order permutation variance (cf. Section "Methods" in the main text). In contrast to the MCM, we do not implement a multi-MLP but use the standard architecture of the GNN, which, in fact, uses the same MLP with one output to make predictions for $\ln(\gamma_1)$ and $\ln(\gamma_2)$ in a sequential manner (cf.[1]), thereby having similar characteristics to the multi-MLP MCM. Again, all models are trained with standard prediction loss and with ReLU as the MLP activation function.

We show the performance histograms on activity coefficient predictions in Figure S2a and on thermodynamic consistency in Figure S2b for the GNN with different MLP architectures. The composition-dependent errors are shown in Figures S2c, S2d. We observe an analogous trend to the MCM: The aggregated prediction accuracies and thermodynamic consistencies are on a similar level for the differ-

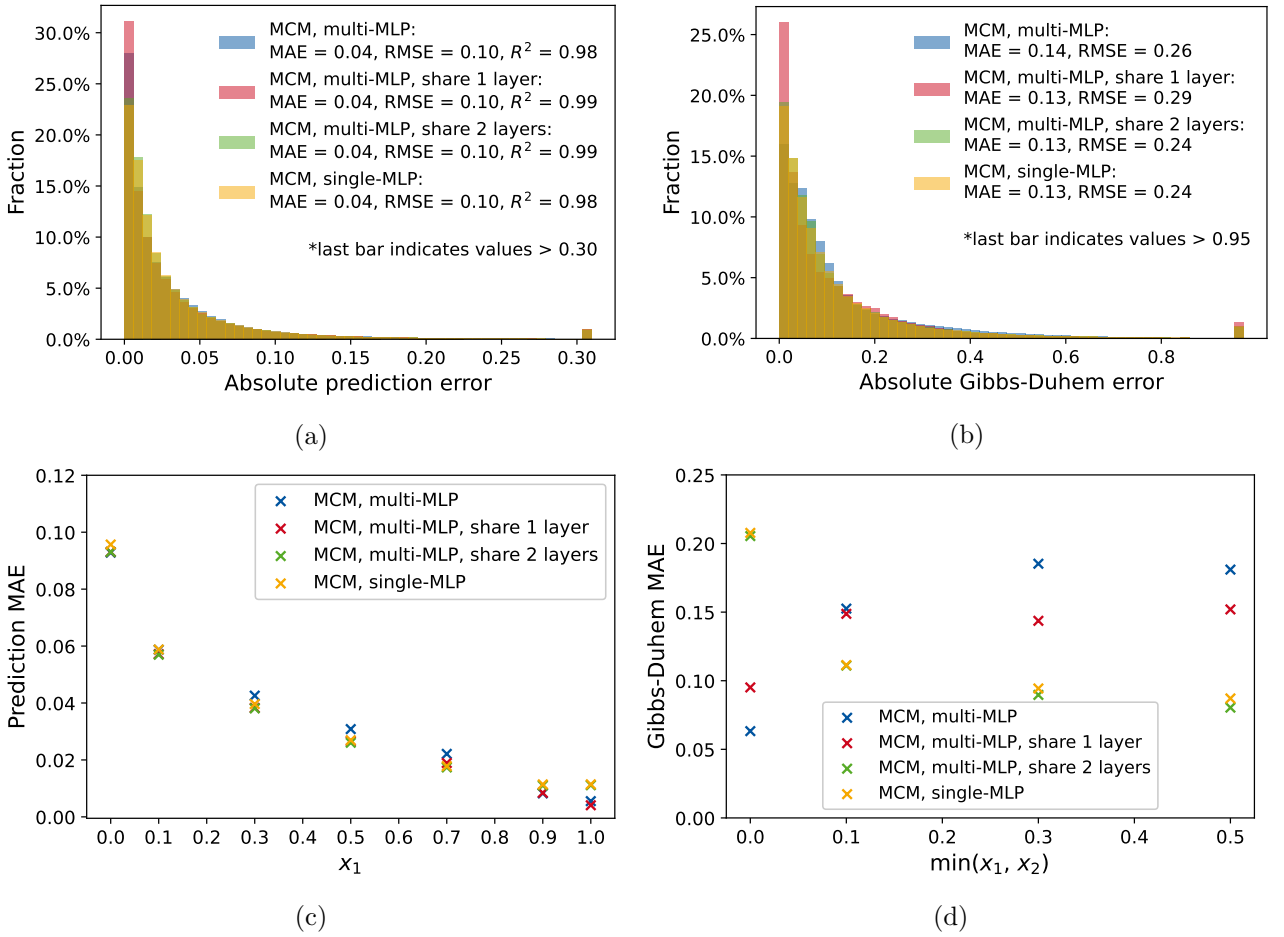

Figure S1: Absolute prediction error and absolute deviation from Gibbs-Duhem differential equation are illustrated in histograms (a,b) and composition-dependent plots (c,d) for MCM with different MLP architectures trained with a standard loss function based on the prediction error and MLP activation function: ReLU. The outlier thresholds (a,b) are determined based on the top 1 % of the highest errors of MCM, multi-MLP.

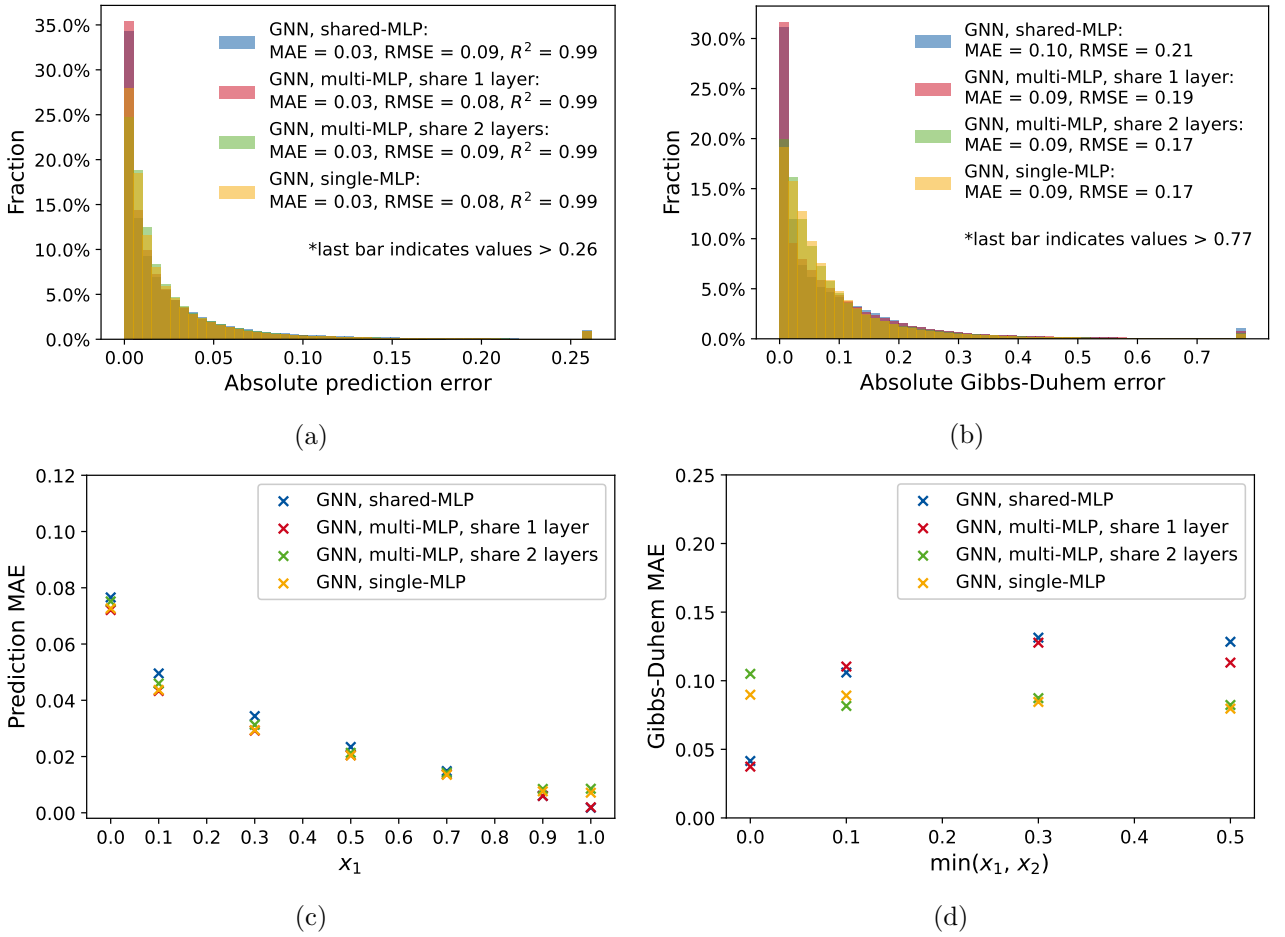

Figure S2: Absolute prediction error and absolute deviation from Gibbs-Duhem differential equation are illustrated in histograms (a,b) and composition-dependent plots (c,d) for the GNN with different MLP architectures trained with a standard loss function based on the prediction error and MLP activation function: ReLU. The outlier thresholds (a,b) are determined based on the top 1 % of highest errors of GNN, shared-MLP.

Table S1: Prediction accuracies and thermodynamic consistencies measured by root mean squared error (RMSE) for comp-inter split (cf. [1]) by the GNN and MCM both with a single-MLP consisting of shared hidden layers and two outputs for $ln(\gamma_1)$ and $ln(\gamma_2)$. The models are trained with different hyperparameters: MLP activation function, Gibbs-Duhem loss weighting factor λ, and data augmentation.

model setup			GNN, single-MLP			MCM, single-MLP		
MLP act.	λ	data augm.	$RMSE_{test}$	GD-$RMSE_{test}$	GD-$RMSE^{ext}_{test}$	$RMSE_{test}$	GD-$RMSE_{test}$	GD-$RMSE^{ext}_{test}$
relu	0.0	False	0.085	0.166	0.193	0.103	0.244	0.189
softplus	0.0	False	0.080	0.099	0.156	0.090	0.176	0.107
	1.0	False	0.076	0.032	0.278	0.089	0.044	0.057
	1.0	True	0.077	0.019	0.022	0.093	0.026	0.024

ent architectures. However, considering the composition-dependent results, we observe that the more intertwined MLPs show higher errors at the boundary compositions, while the separated MLPs show higher errors at the intermediate compositions.

We further tested Gibbs-Duhem-informed neural networks with different MLP architectures on the comp-inter split (cf. Section "Data set" in the main text). Table S1 shows the results for the SolvGNN and MCM both having a single-MLP trained without and with Gibbs-Duhem loss. Similar to the results presented in Section "Gibbs-Duhem-informed training" of the main text, we observe that training with Gibbs-Duhem loss, here $\lambda = 1$, and data augmentation can significantly increase the thermodynamic consistency at similar levels of prediction accuracies compared to the models trained without Gibbs-Duhem loss ($\lambda = 0$). The results for varying MLP architectures, therefore, substantiate the effectiveness of Gibbs-Duhem-informed neural networks.

Overall, our results thus indicate that the structure of the prediction MLP can have an influence on the composition-dependent thermodynamic consistency, with Gibbs-Duhem-informed training being beneficial independent of the MLP structure. It would be interesting to further investigate the effects of the MLP structure on the Gibbs-Duhem consistency in future work.

2 Additional comparison of different activation functions

We show additional illustrations for comparing different activation functions, namely, ReLU, ELU, and softplus. Specifically, we show comparisons of the different activations functions used in the MLP of the GNN, the MCM, and the GNN_{xMLP}, receptively, for the comp-inter split and considering three different training setups: Figure S3: $\lambda = 0$, Figure S4: $\lambda = 1$ without data augmentation, Figure S5: $\lambda = 1$ with data augmentation. The results correspond to Table 1 of the main text.

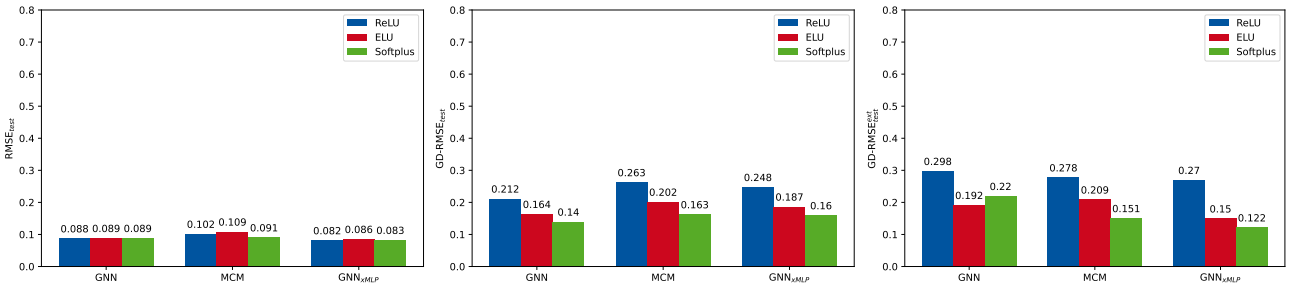

(a) (b) (c)

Figure S3: Prediction accuracy (a) and thermodynamic consistency (b, c) for GNN, MCM, and GNN_{xMLP} trained with a standard loss function, i.e., $\lambda = 0$, and with different MLP activation functions.

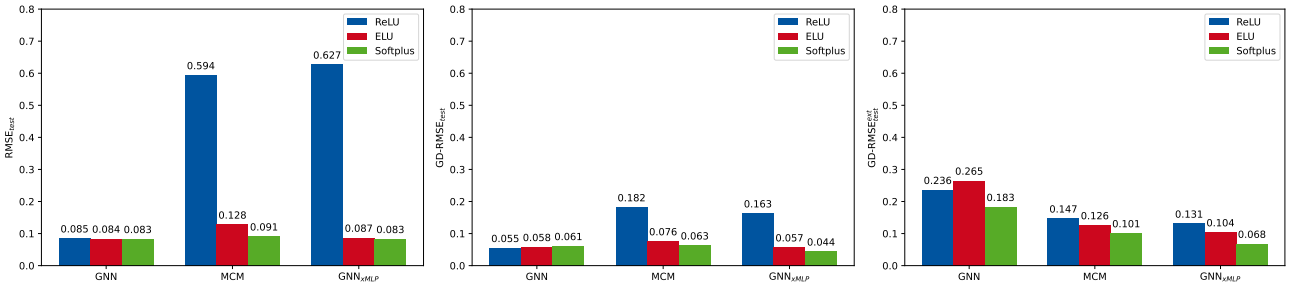

(a) (b) (c)

Figure S4: Prediction accuracy (a) and thermodynamic consistency (b, c) for GNN, MCM, and GNN_{xMLP} trained with Gibbs-Duhem-informed loss function and following hyperparameters: weighting factor $\lambda = 1$, data augmentation: false, and with different MLP activation functions.

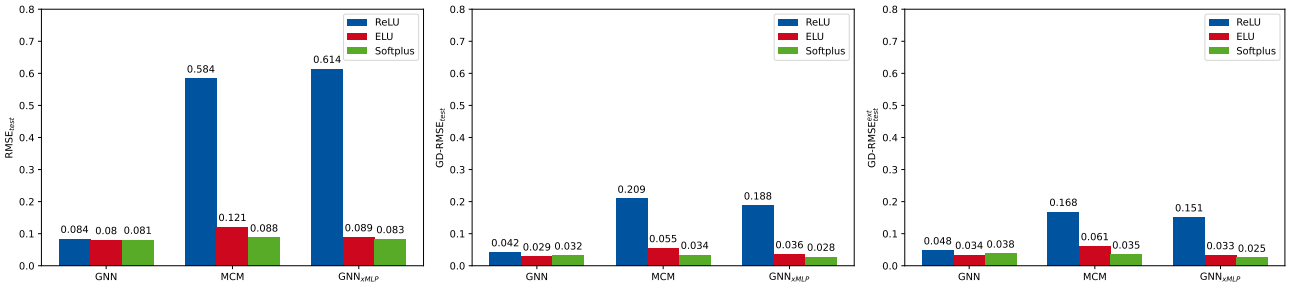

(a) (b) (c)

Figure S5: Prediction accuracy (a) and thermodynamic consistency (b, c) for GNN, MCM, and GNN_{xMLP} trained with Gibbs-Duhem-informed loss function and following hyperparameters: weighting factor $\lambda = 1$, data augmentation: true, and with different MLP activation functions.

3 Additional activity coefficient predictions with gradients

We provide further activity coefficient predictions and the corresponding composition-dependent gradients with the evaluation of the Gibbs-Duhem differential constraint for the GNN, MCM, and $\mathrm{GNN_{xMLP}}$. Specifically, we show the ensemble results for the comp-inter split not presented in the main text and further show the individual models for each of the five training runs associated with the comp-inter split. The results shown in Section 3.1 correspond to models trained with the following hyperparameters: MLP activation function: ReLU, weighting factor $\lambda = 0$, data augmentation: false. The results shown in Section 3.2 correspond to models trained with the following hyperparameters: MLP activation function: softplus, weighting factor $\lambda = 1$, data augmentation: true; in Section 3.3, we also show the ensemble results with the same setup but data augmentation: false.

3.1 Standard training

GNN:

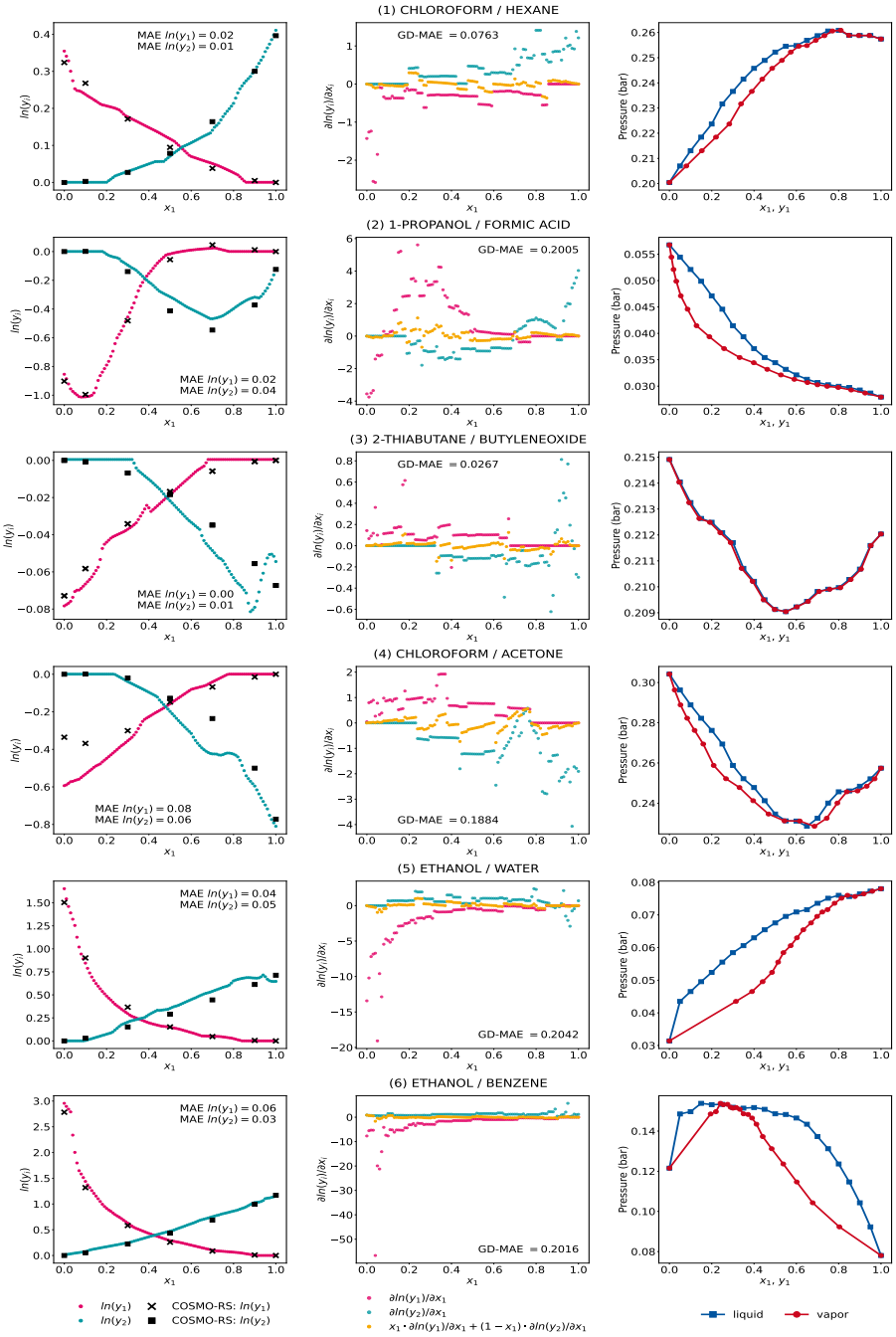

Figure S6: Activity coefficient predictions and their corresponding gradients with respect to the composition and the associated Gibbs-Duhem deviations for exemplary mixtures by the GNN trained with standard loss function and following hyperparameters: MLP activation function: ReLU, weighting factor $\lambda = 0$, data augmentation: false. Results are from **run 1** of comp-inter split.

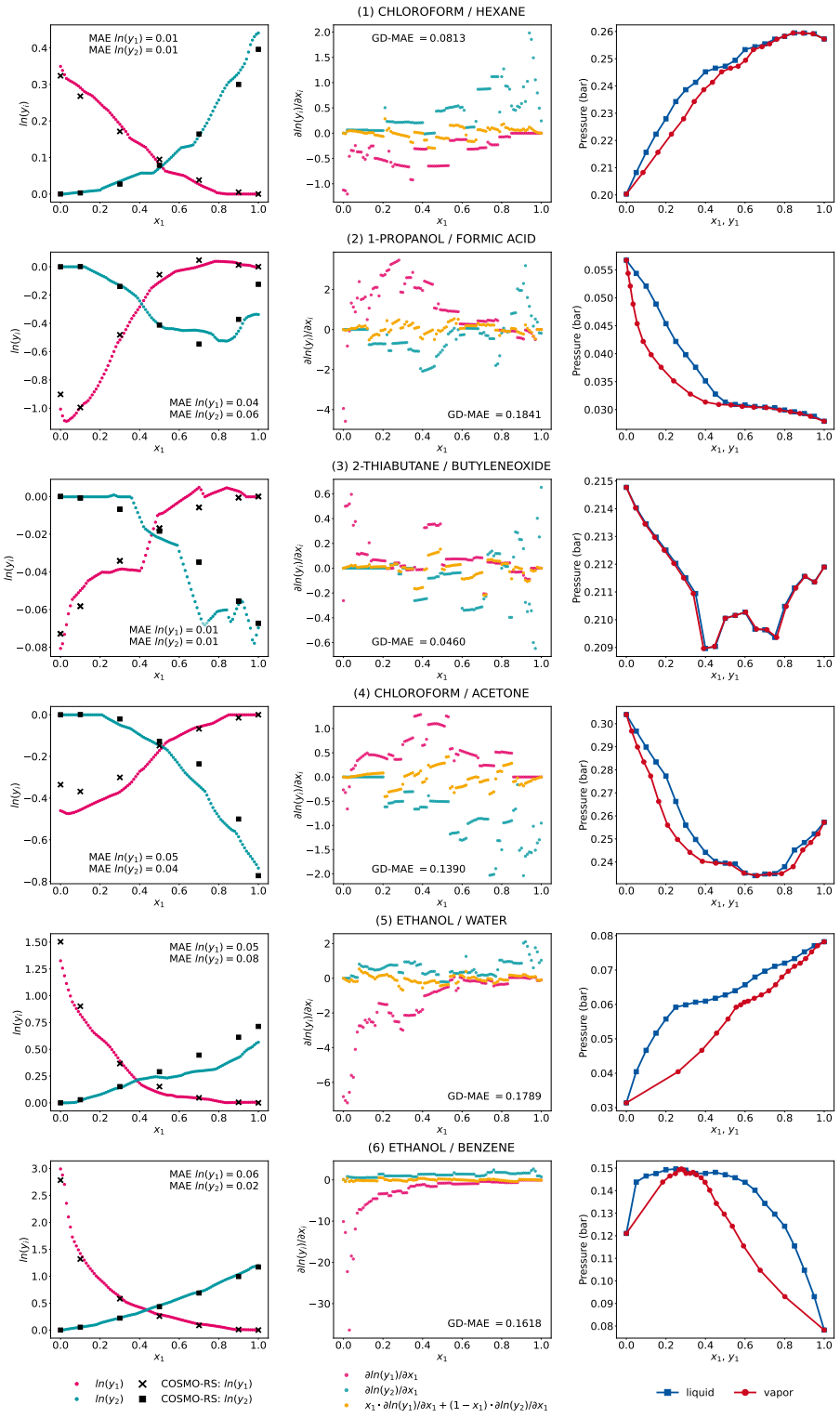

Figure S7: Activity coefficient predictions and their corresponding gradients with respect to the composition and the associated Gibbs-Duhem deviations for exemplary mixtures by the GNN trained with standard loss function and following hyperparameters: MLP activation function: ReLU, weighting factor $\lambda = 0$, data augmentation: false. Results are from **run 2** of comp-inter split.

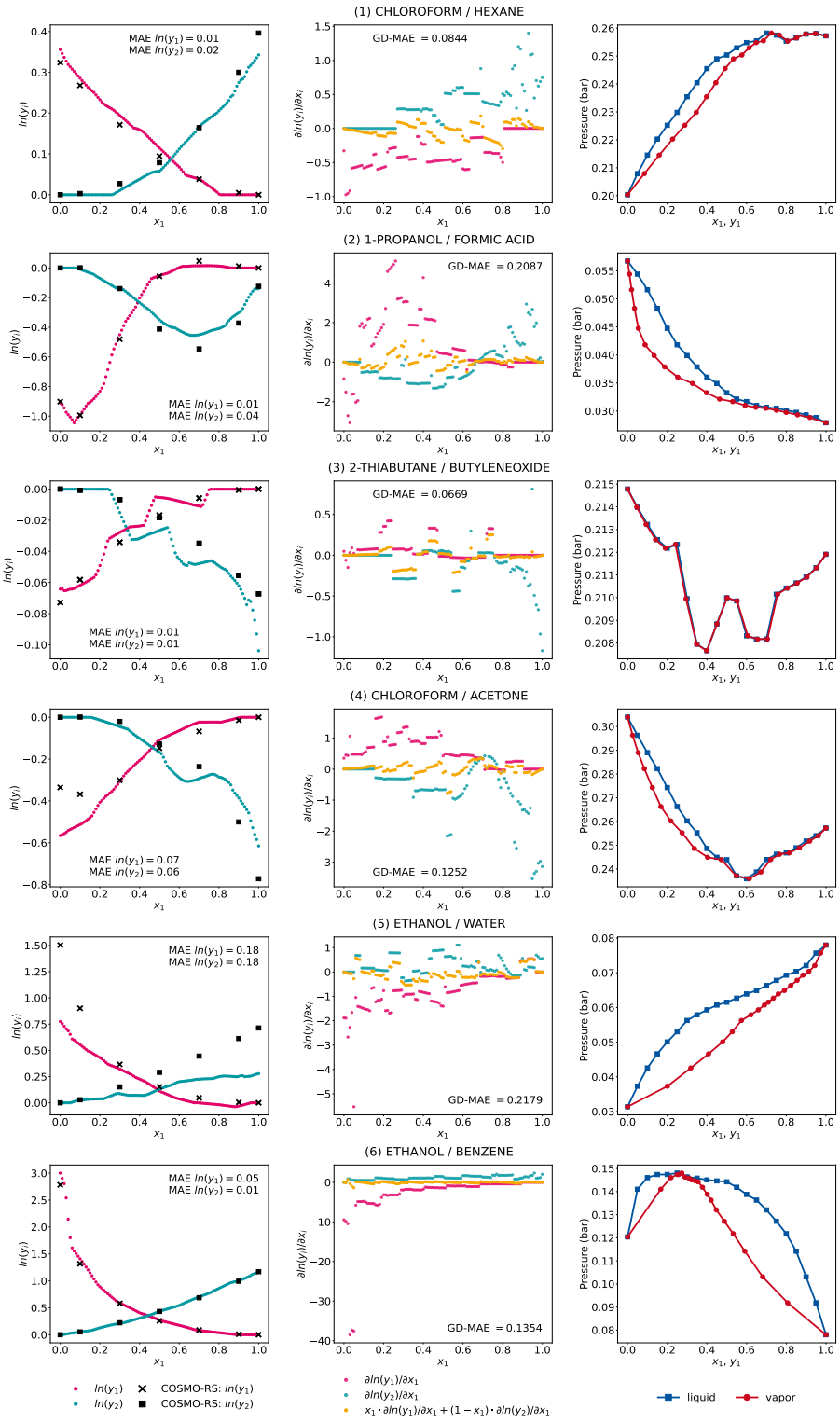

Figure S8: Activity coefficient predictions and their corresponding gradients with respect to the composition and the associated Gibbs-Duhem deviations for exemplary mixtures by the GNN trained with standard loss function and following hyperparameters: MLP activation function: ReLU, weighting factor $\lambda = 0$, data augmentation: false. Results are from **run 3** of comp-inter split.

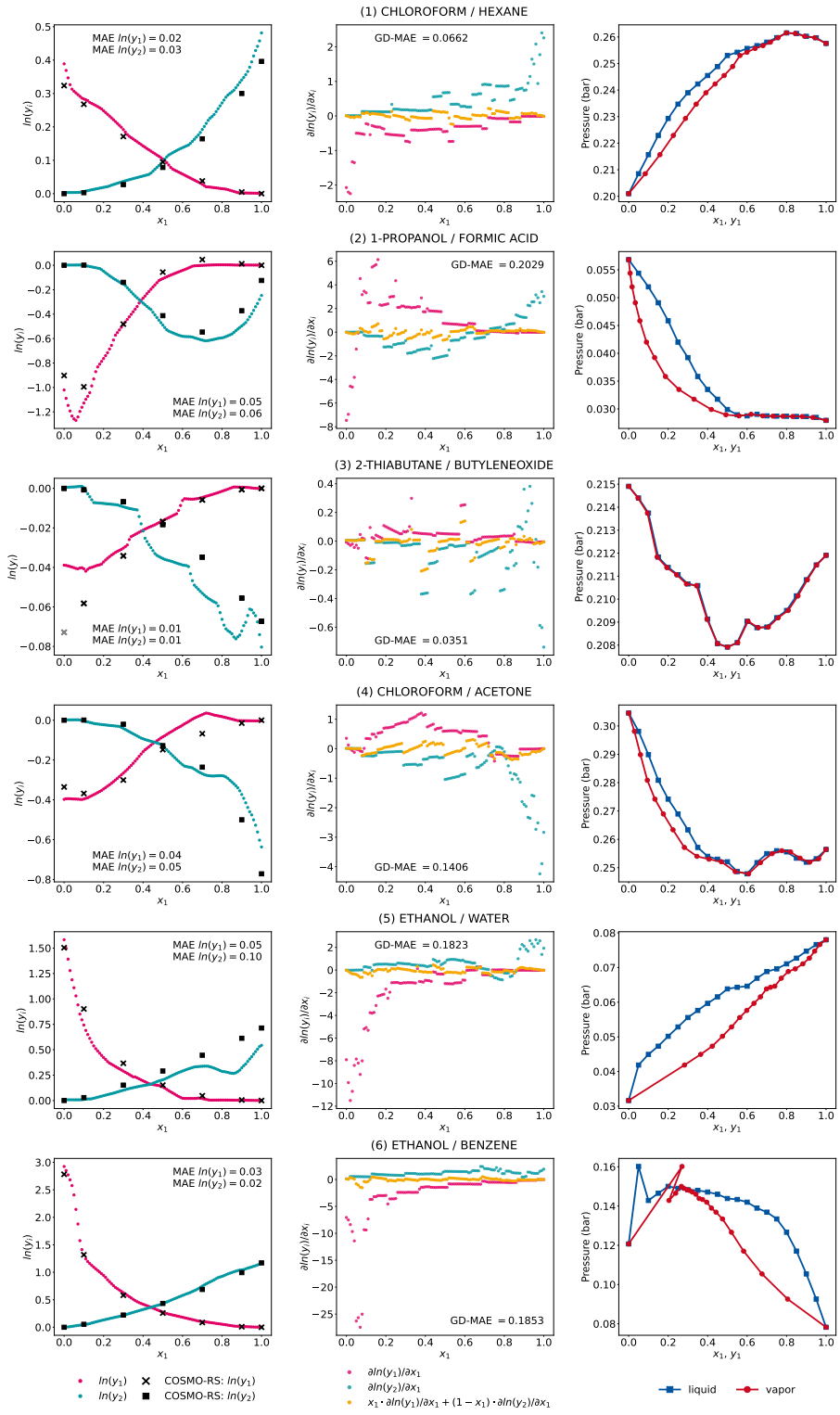

Figure S9: Activity coefficient predictions and their corresponding gradients with respect to the composition and the associated Gibbs-Duhem deviations for exemplary mixtures by the GNN trained with standard loss function and following hyperparameters: MLP activation function: ReLU, weighting factor $\lambda = 0$, data augmentation: false. Results are from **run 4** of comp-inter split.

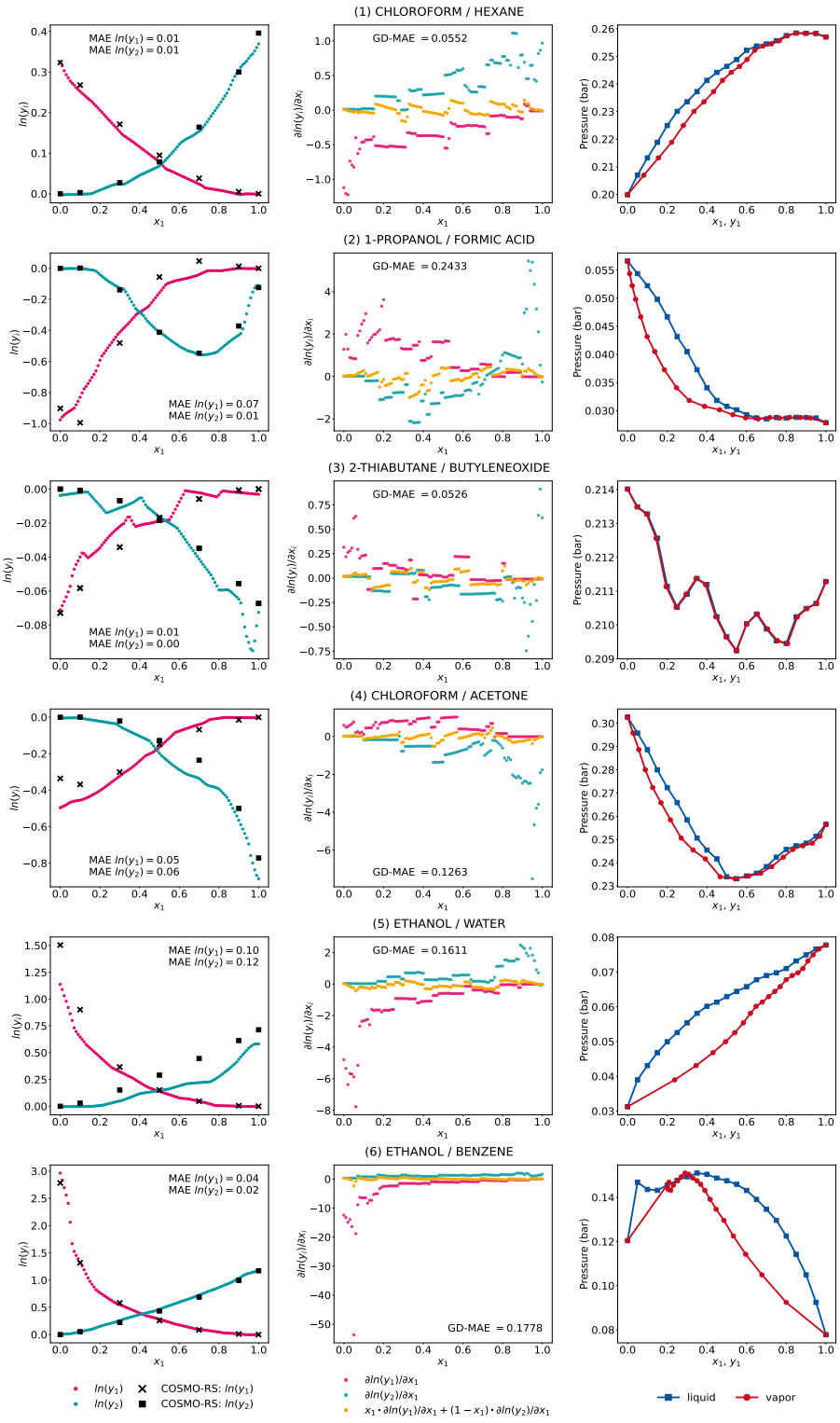

Figure S10: Activity coefficient predictions and their corresponding gradients with respect to the composition and the associated Gibbs-Duhem deviations for exemplary mixtures by the GNN trained with standard loss function and following hyperparameters: MLP activation function: ReLU, weighting factor $\lambda = 0$, data augmentation: false. Results are from **run 5** of comp-inter split.

MCM:

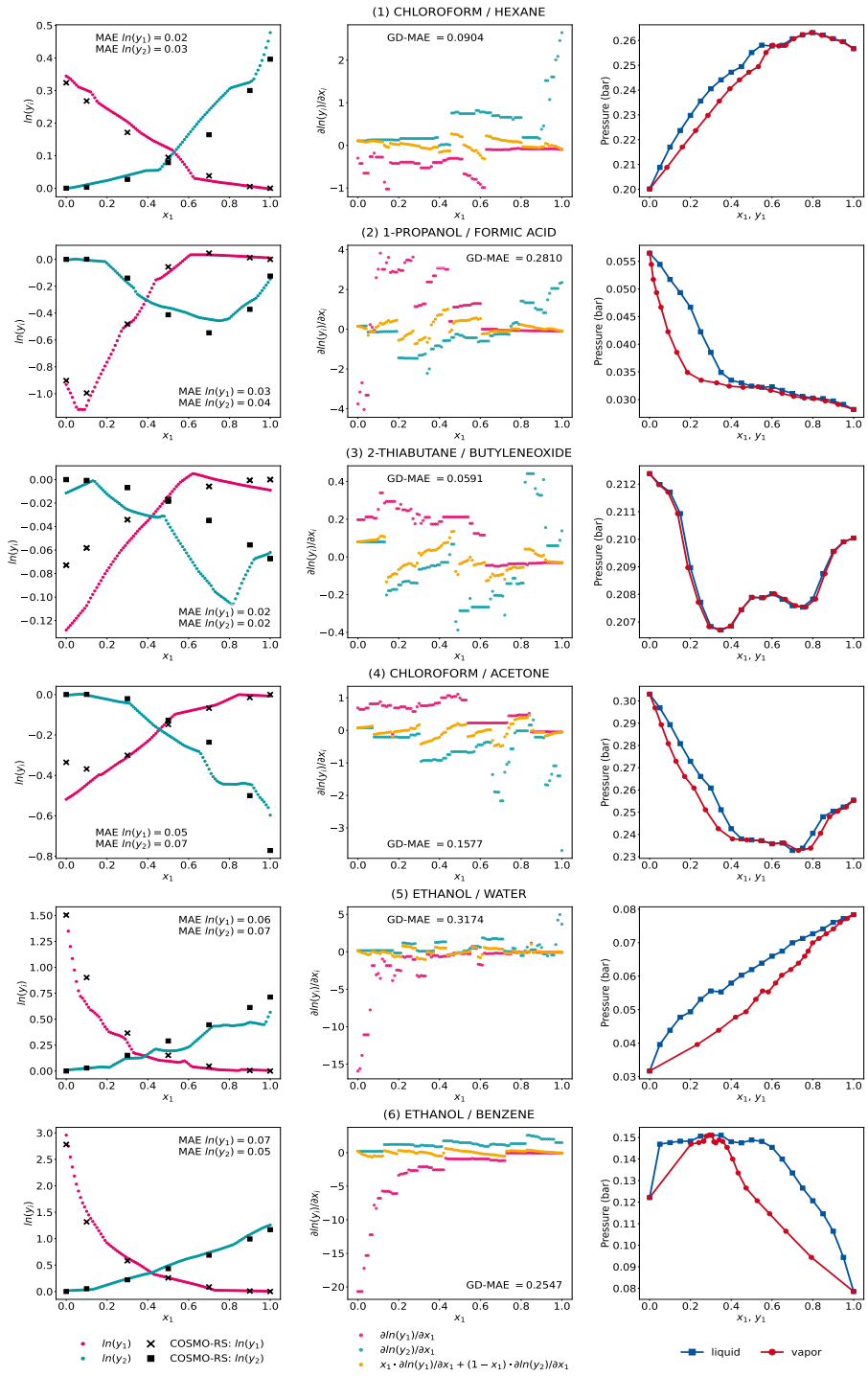

Figure S11: Activity coefficient predictions and their corresponding gradients with respect to the composition and the associated Gibbs-Duhem deviations for exemplary mixtures by MCM trained with standard loss function and following hyperparameters: MLP activation function: ReLU, weighting factor $\lambda = 0$, data augmentation: false. Results are from **run 1** of comp-inter split.

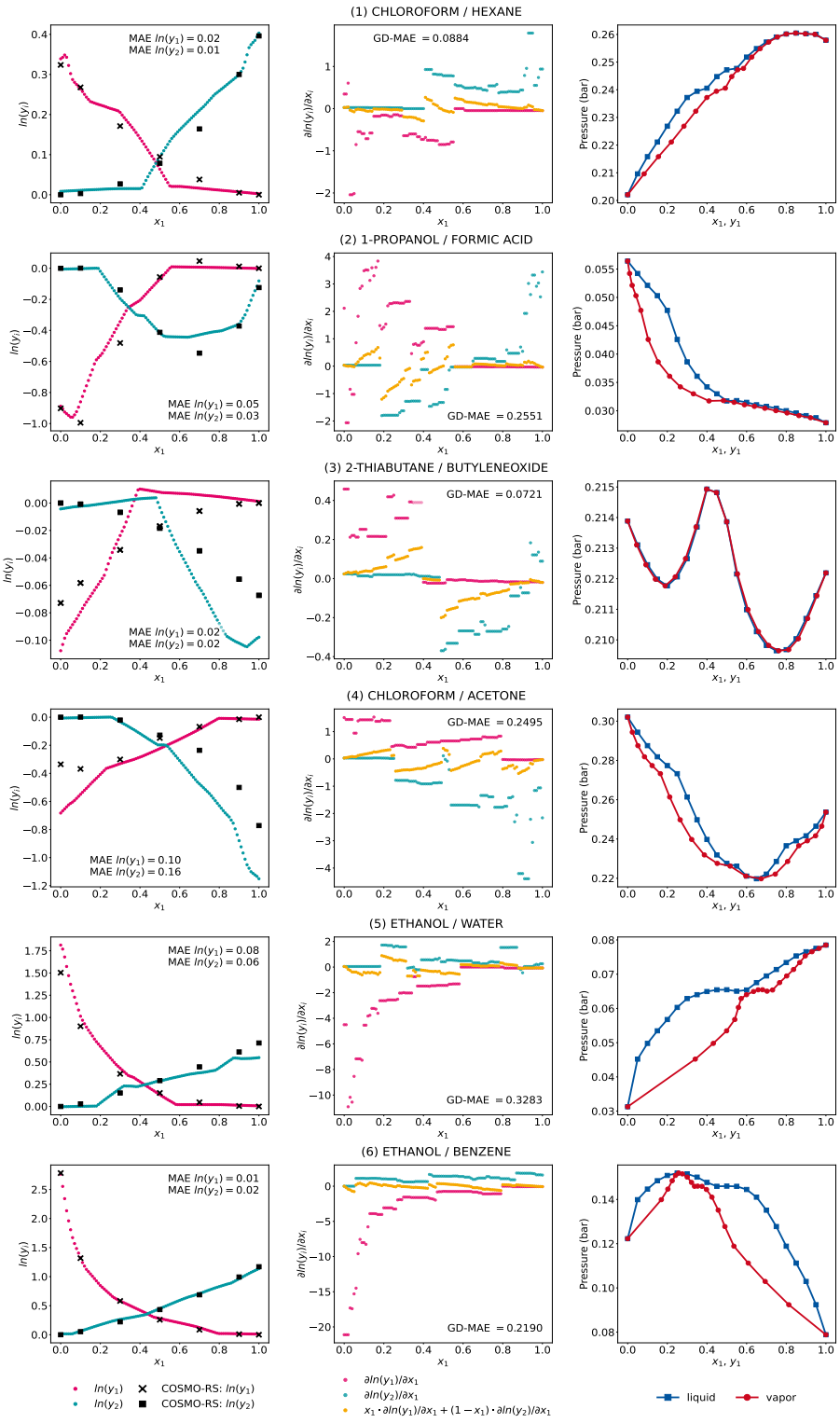

Figure S12: Activity coefficient predictions and their corresponding gradients with respect to the composition and the associated Gibbs-Duhem deviations for exemplary mixtures by MCM trained with standard loss function and following hyperparameters: MLP activation function: ReLU, weighting factor $\lambda = 0$, data augmentation: false. Results are from **run 2** of comp-inter split.

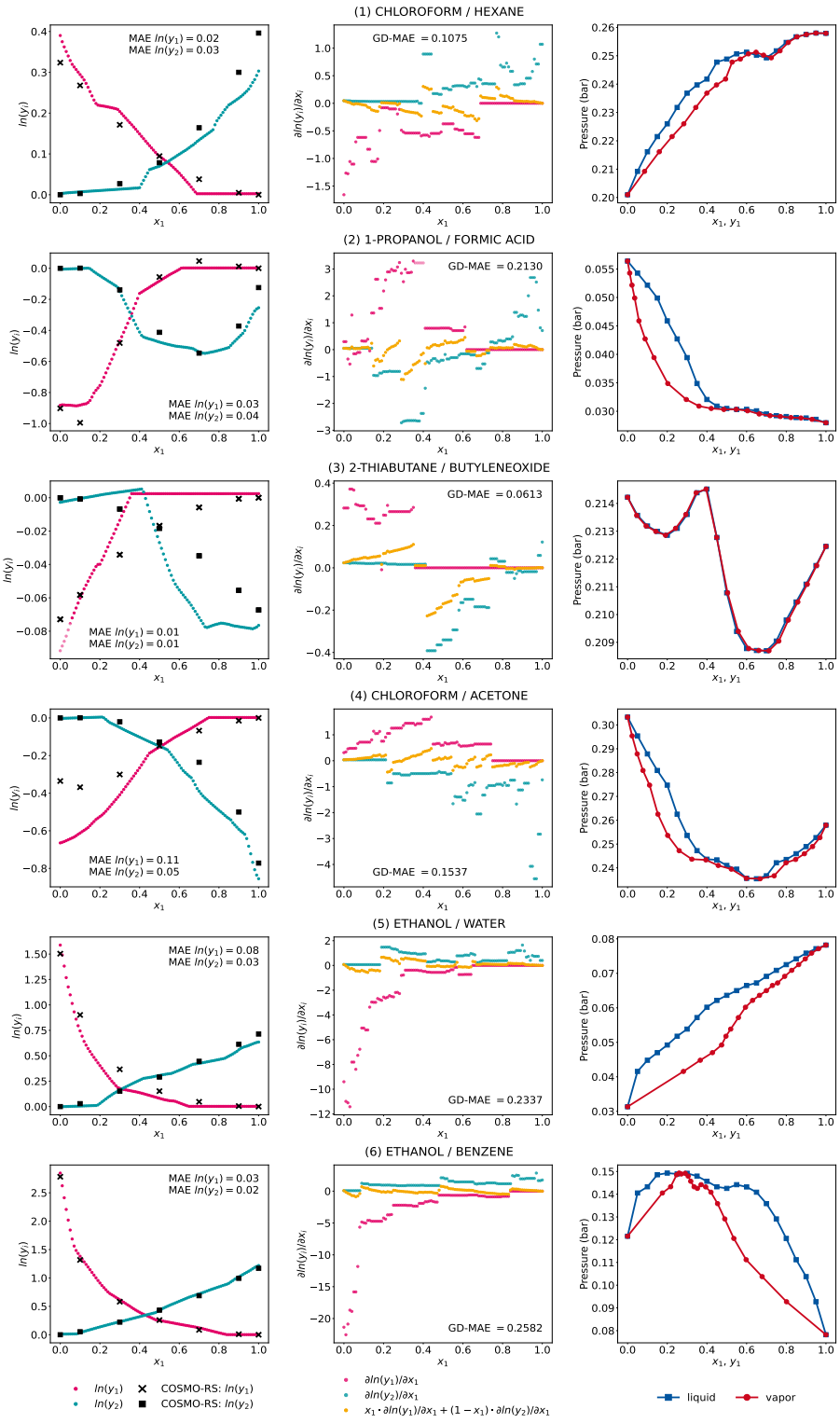

Figure S13: Activity coefficient predictions and their corresponding gradients with respect to the composition and the associated Gibbs-Duhem deviations for exemplary mixtures by MCM trained with standard loss function and following hyperparameters: MLP activation function: ReLU, weighting factor $\lambda = 0$, data augmentation: false. Results are from **run 3** of comp-inter split.

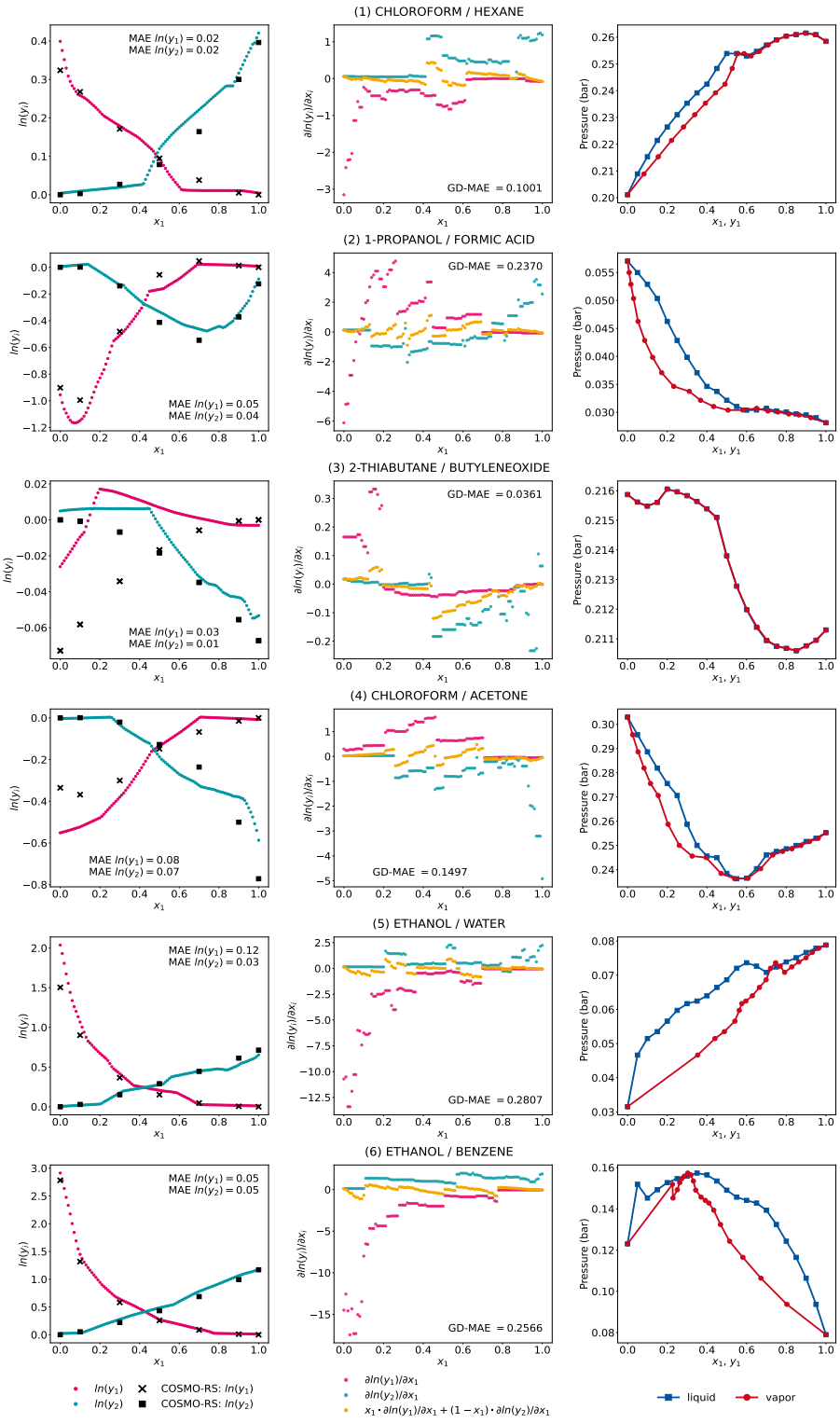

Figure S14: Activity coefficient predictions and their corresponding gradients with respect to the composition and the associated Gibbs-Duhem deviations for exemplary mixtures by MCM trained with standard loss function and following hyperparameters: MLP activation function: ReLU, weighting factor $\lambda = 0$, data augmentation: false. Results are from **run 4** of comp-inter split.

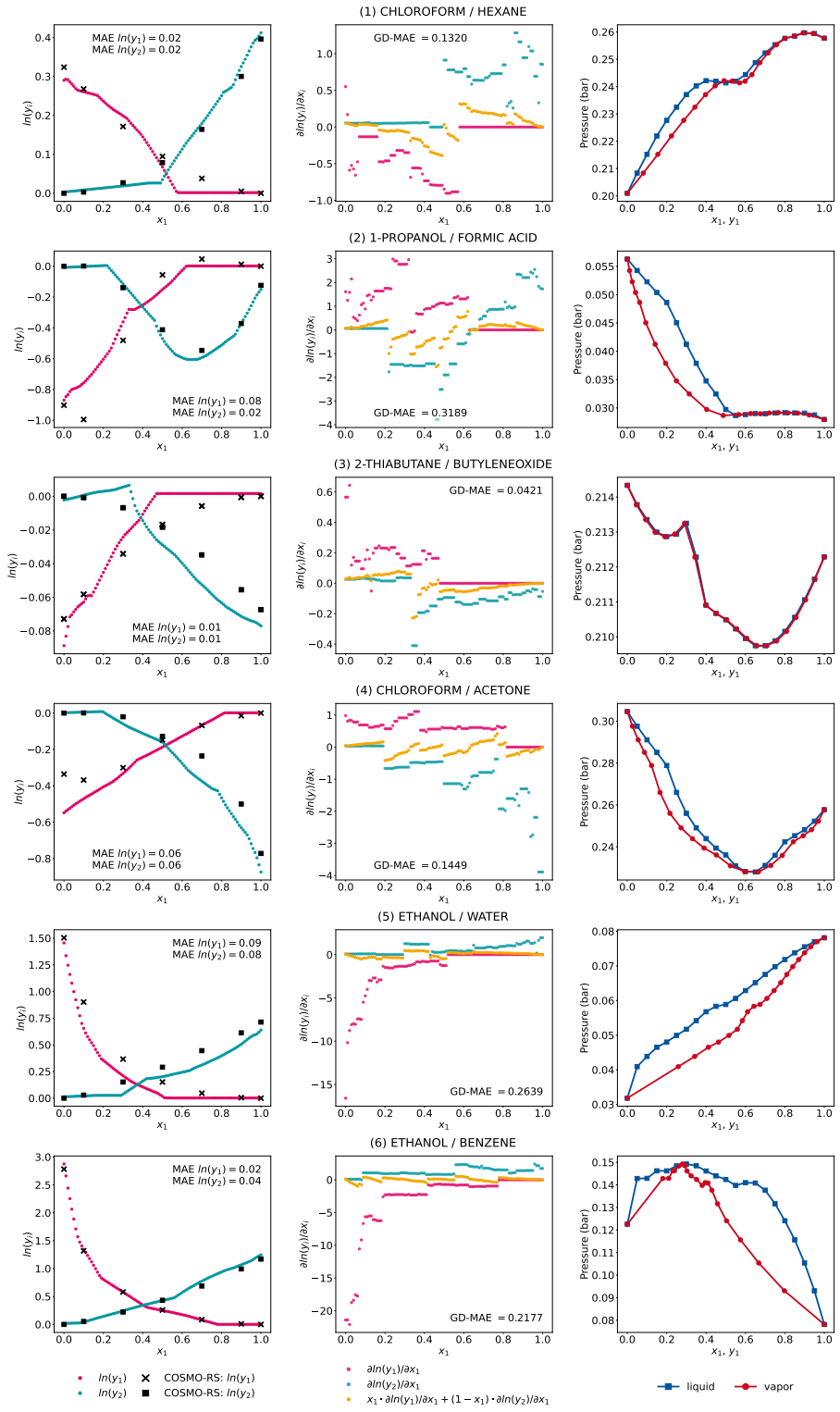

Figure S15: Activity coefficient predictions and their corresponding gradients with respect to the composition and the associated Gibbs-Duhem deviations for exemplary mixtures by MCM trained with standard loss function and following hyperparameters: MLP activation function: ReLU, weighting factor $\lambda = 0$, data augmentation: false. Results are from **run 5** of comp-inter split.

GNN_{xMLP}:

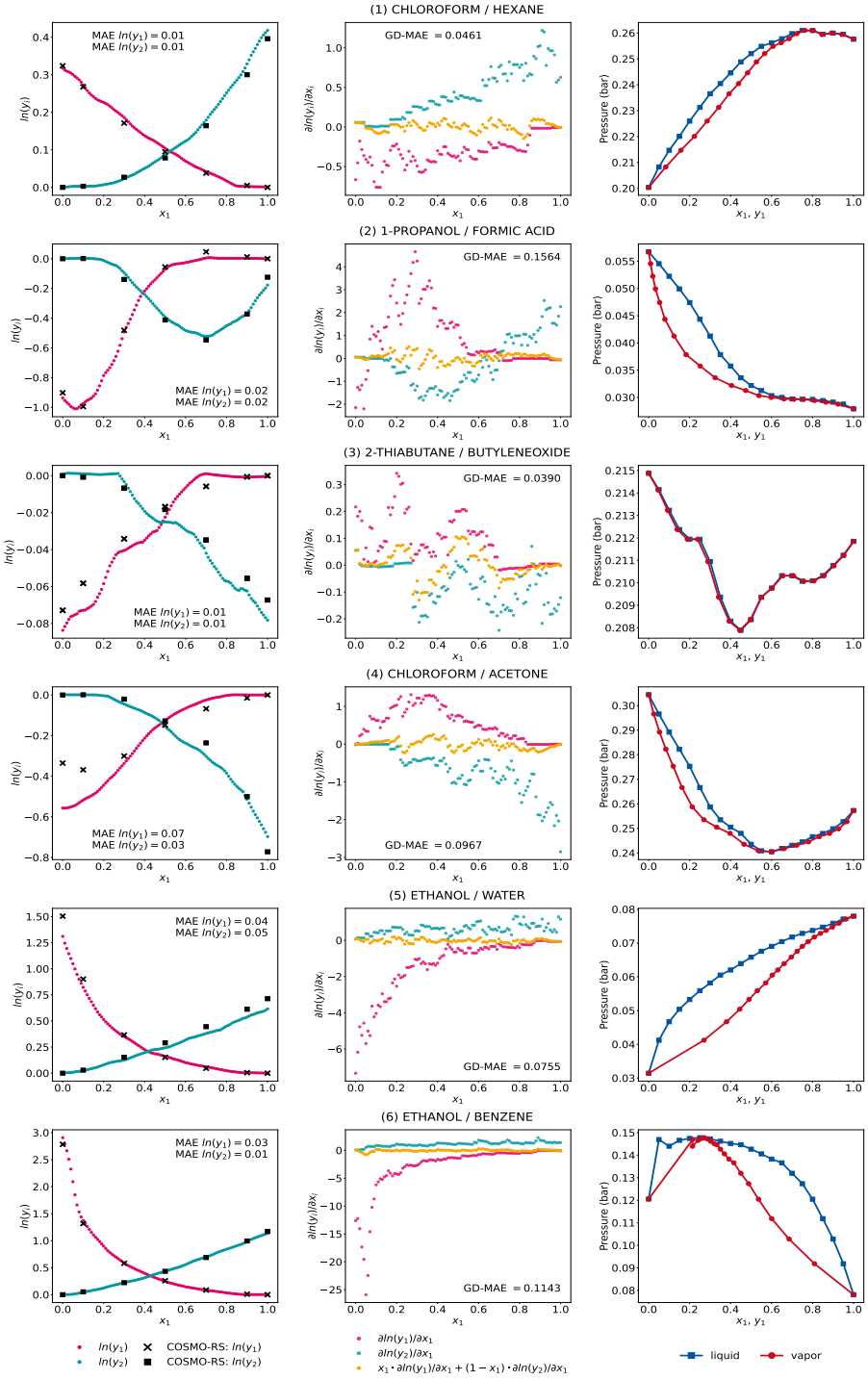

Figure S16: Activity coefficient predictions and their corresponding gradients with respect to the composition and the associated Gibbs-Duhem deviations for exemplary mixtures by the GNN_{xMLP} ensemble trained with standard loss function and following hyperparameters: MLP activation function: ReLU, weighting factor $\lambda = 0$, data augmentation: false. Results are averaged from the five model runs of the comp-inter split.

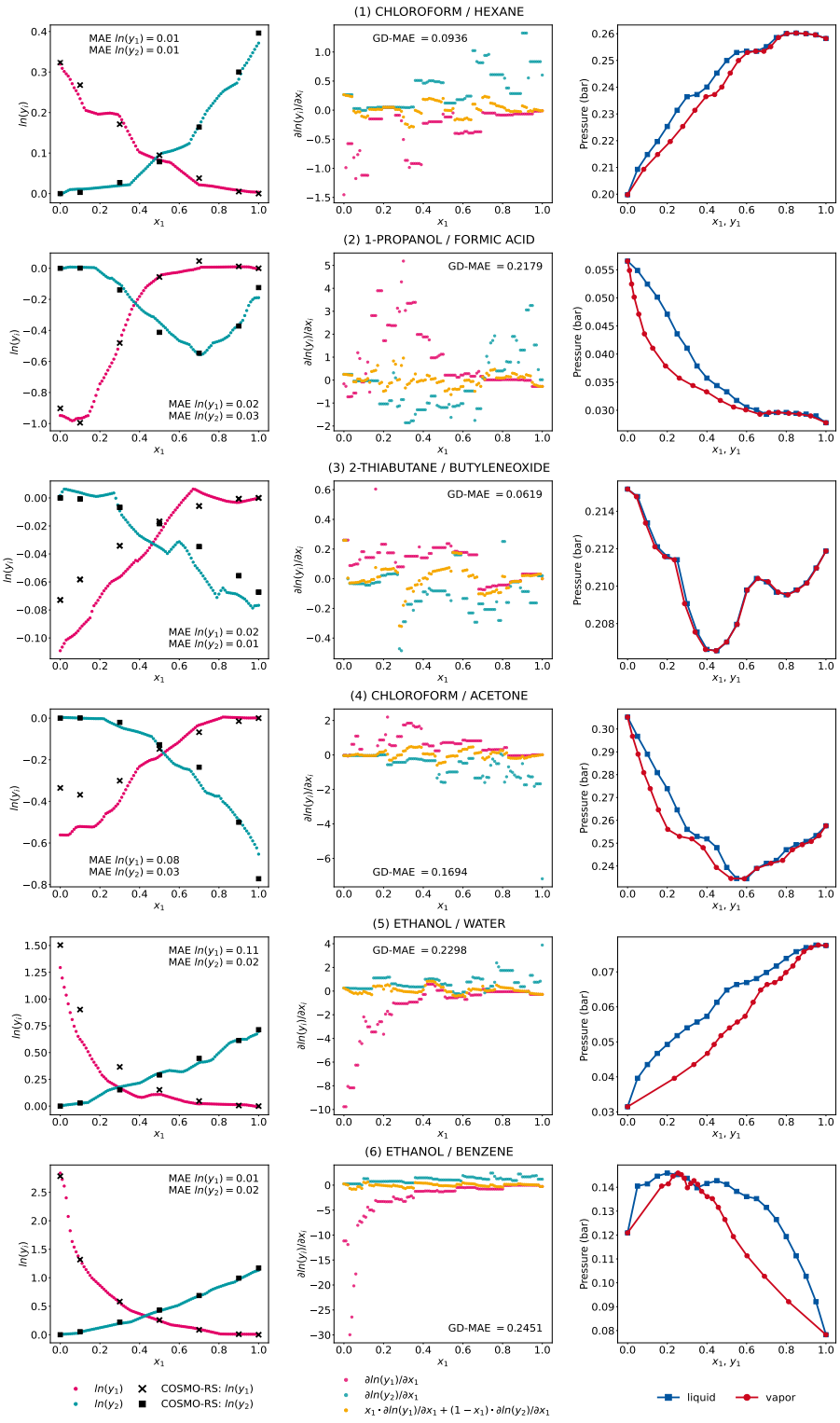

Figure S17: Activity coefficient predictions and their corresponding gradients with respect to the composition and the associated Gibbs-Duhem deviations for exemplary mixtures by the GNN_{xMLP} trained with standard loss function and following hyperparameters: MLP activation function: ReLU, weighting factor $\lambda = 0$, data augmentation: false. Results are from **run 1** of comp-inter split.

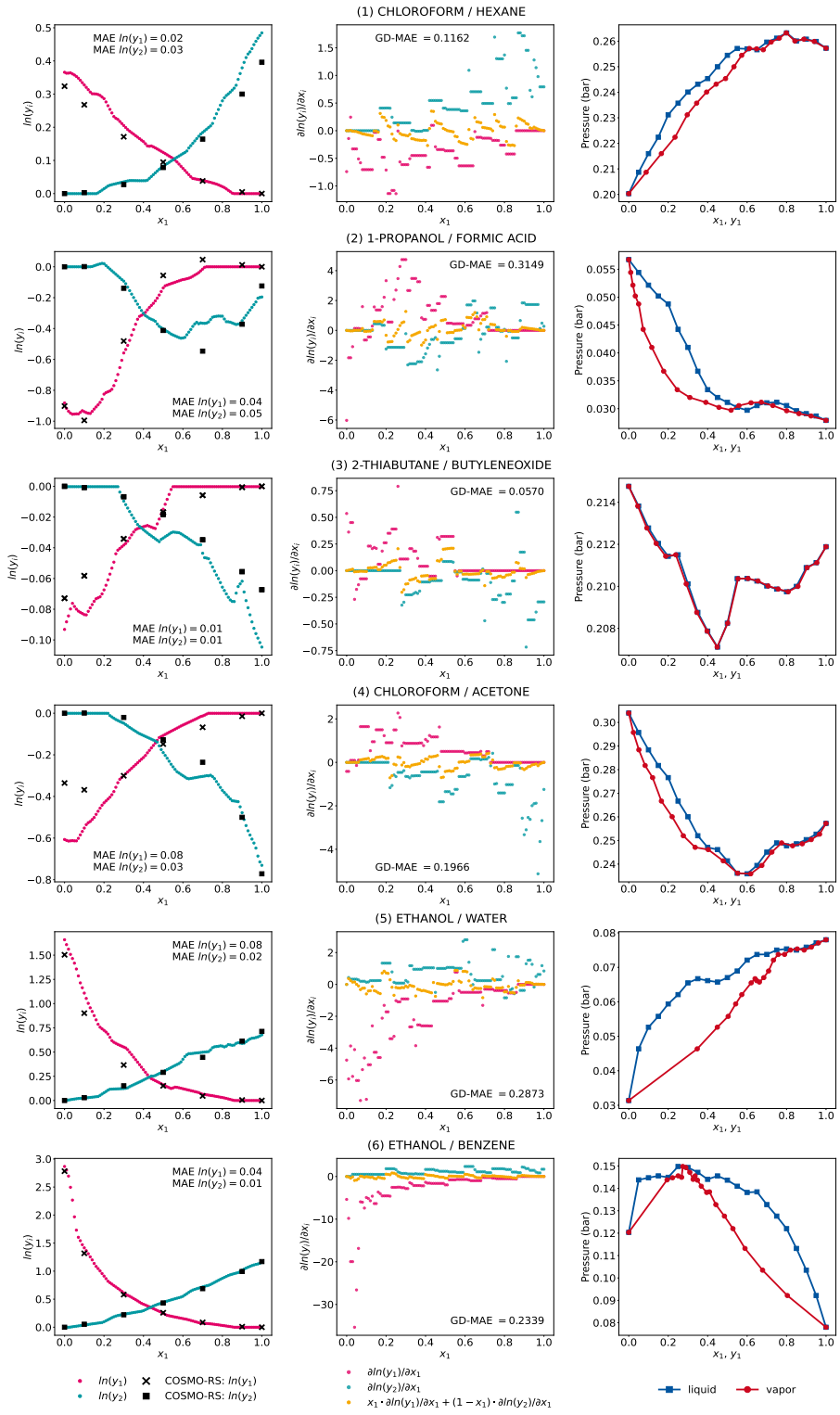

Figure S18: Activity coefficient predictions and their corresponding gradients with respect to the composition and the associated Gibbs-Duhem deviations for exemplary mixtures by the GNN_{xMLP} trained with standard loss function and following hyperparameters: MLP activation function: ReLU, weighting factor $\lambda = 0$, data augmentation: false. Results are from **run 2** of comp-inter split.

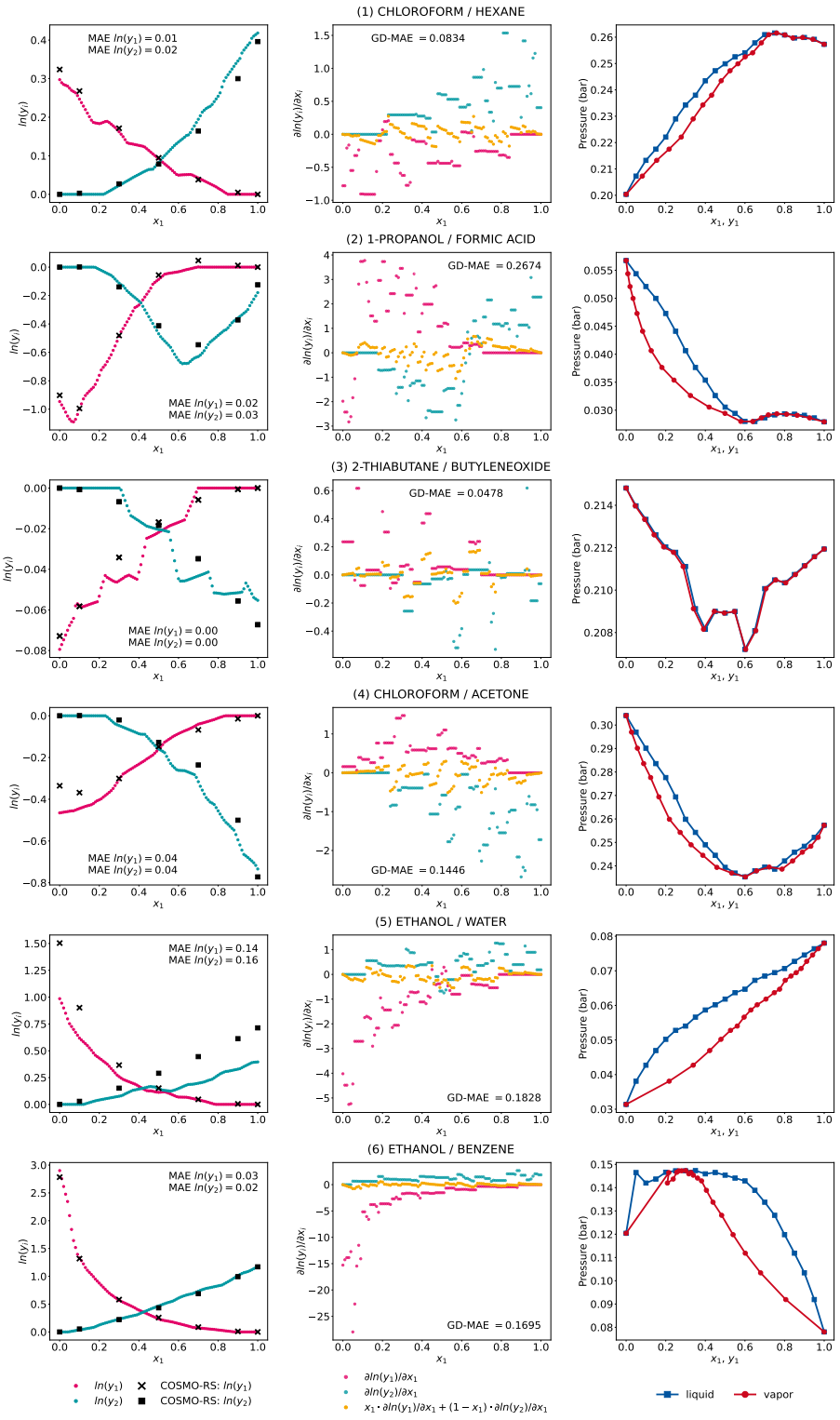

Figure S19: Activity coefficient predictions and their corresponding gradients with respect to the composition and the associated Gibbs-Duhem deviations for exemplary mixtures by the GNN trained with standard loss function and following hyperparameters: MLP activation function: ReLU, weighting factor $\lambda = 0$, data augmentation: false. Results are from **run 3** of comp-inter split.

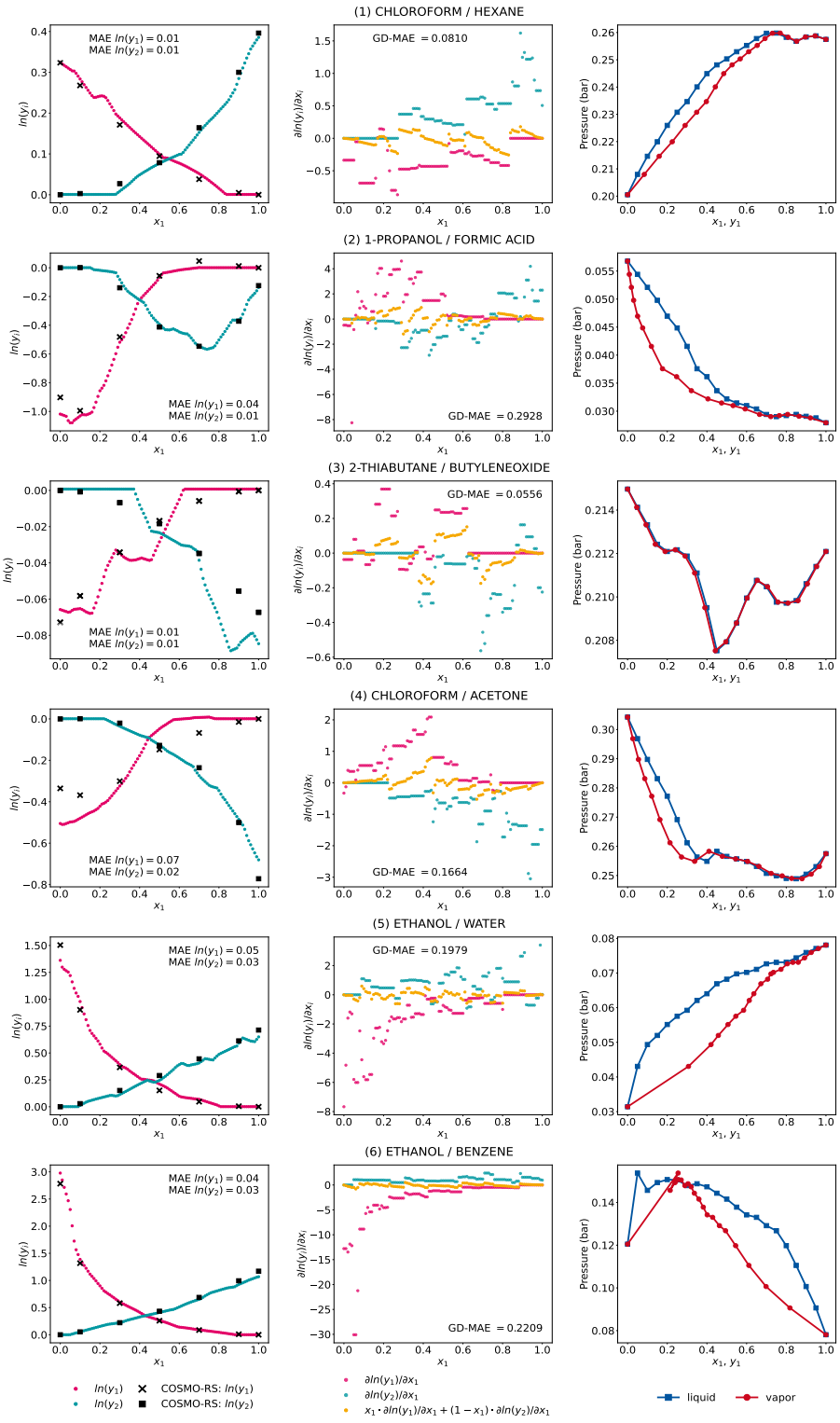

Figure S20: Activity coefficient predictions and their corresponding gradients with respect to the composition and the associated Gibbs-Duhem deviations for exemplary mixtures by the GNN_{xMLP} trained with standard loss function and following hyperparameters: MLP activation function: ReLU, weighting factor $\lambda = 0$, data augmentation: false. Results are from **run 4** of comp-inter split.

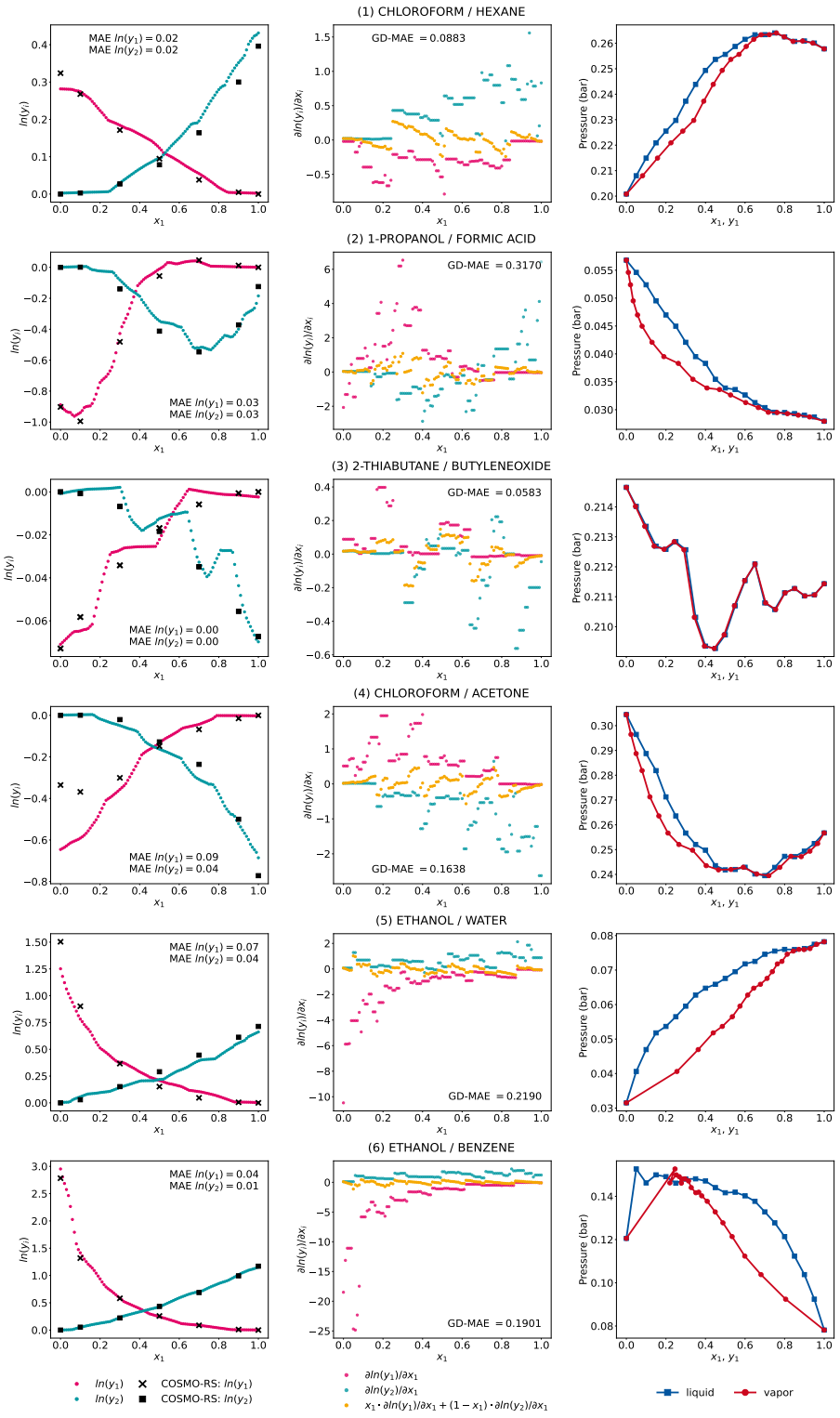

Figure S21: Activity coefficient predictions and their corresponding gradients with respect to the composition and the associated Gibbs-Duhem deviations for exemplary mixtures by the GNN_{xMLP} trained with standard loss function and following hyperparameters: MLP activation function: ReLU, weighting factor $\lambda = 0$, data augmentation: false. Results are from **run 5** of comp-inter split.

3.2 Gibbs-Duhem-informed training with data augmentation

GDI-GNN:

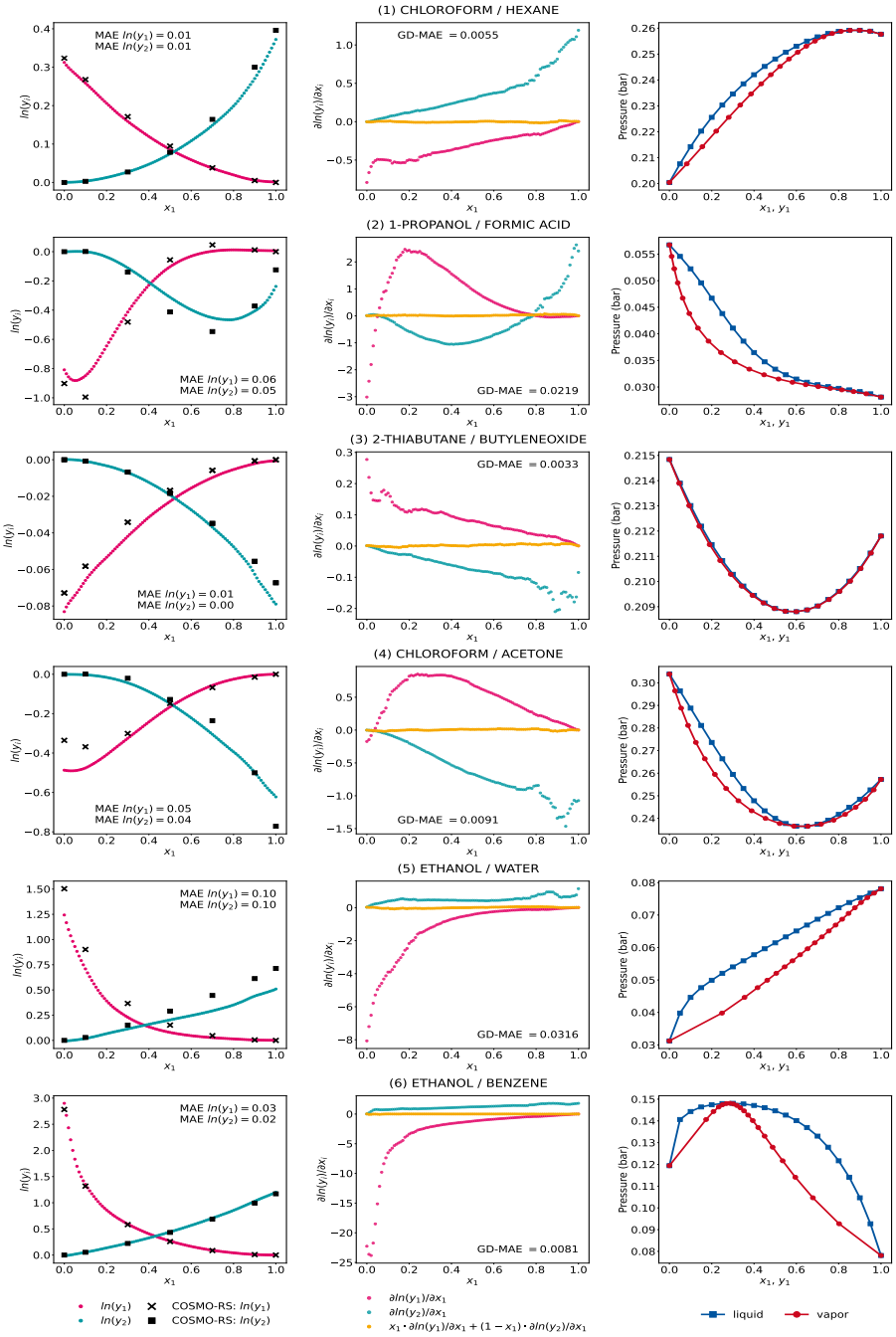

Figure S22: Activity coefficient predictions and their corresponding gradients with respect to the composition and the associated Gibbs-Duhem deviations for exemplary mixtures by the GNN ensemble trained with Gibbs-Duhem-informed loss function and following hyperparameters: MLP activation function: softplus, weighting factor $\lambda = 1$, data augmentation: true. Results are averaged from the five model runs of the comp-inter split.

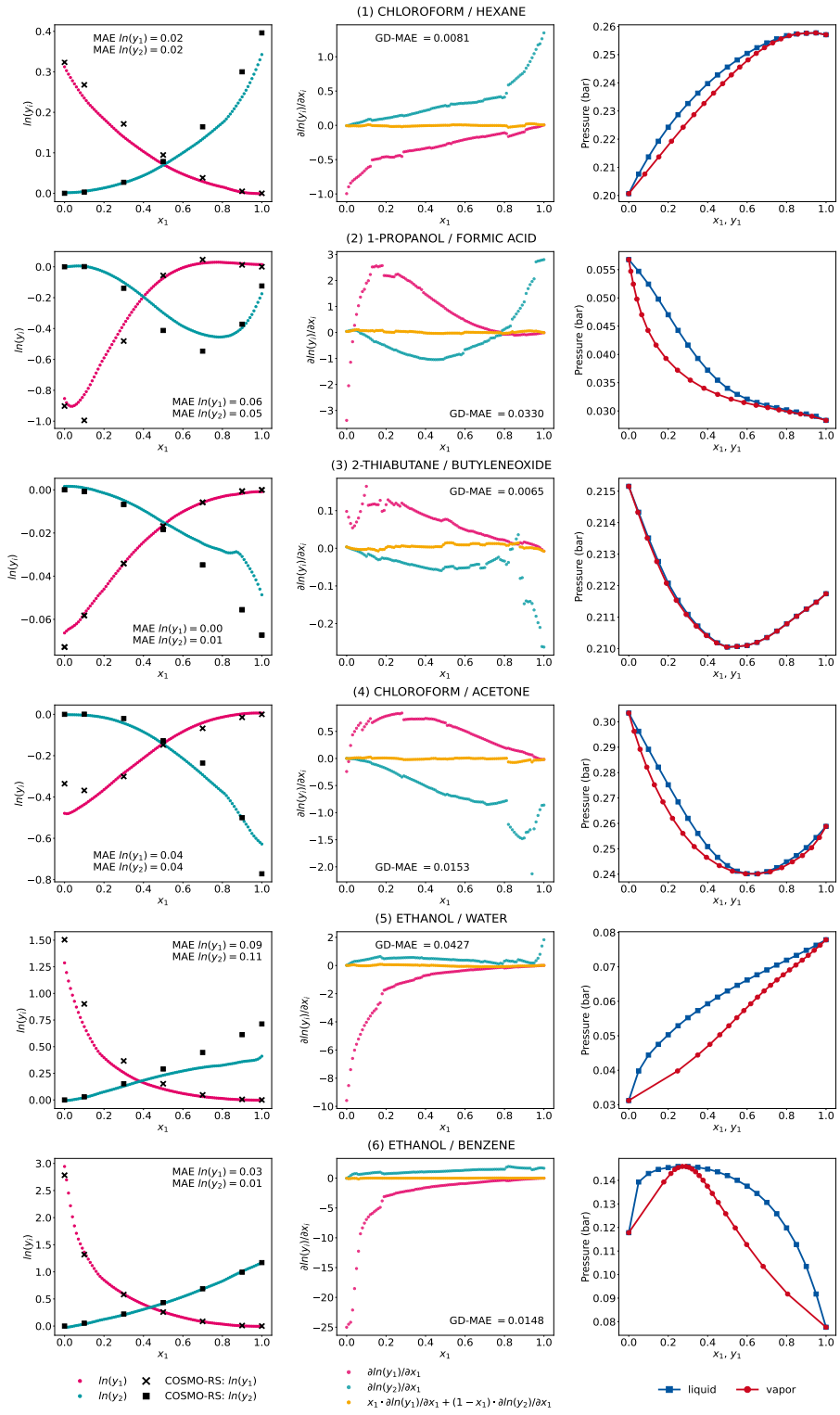

Figure S23: Activity coefficient predictions and their corresponding gradients with respect to the composition and the associated Gibbs-Duhem deviations for exemplary mixtures by the GNN trained with Gibbs-Duhem-informed loss function and following hyperparameters: MLP activation function: softplus, weighting factor $\lambda = 1$, data augmentation: true. Results are from **run 1** of comp-inter split.

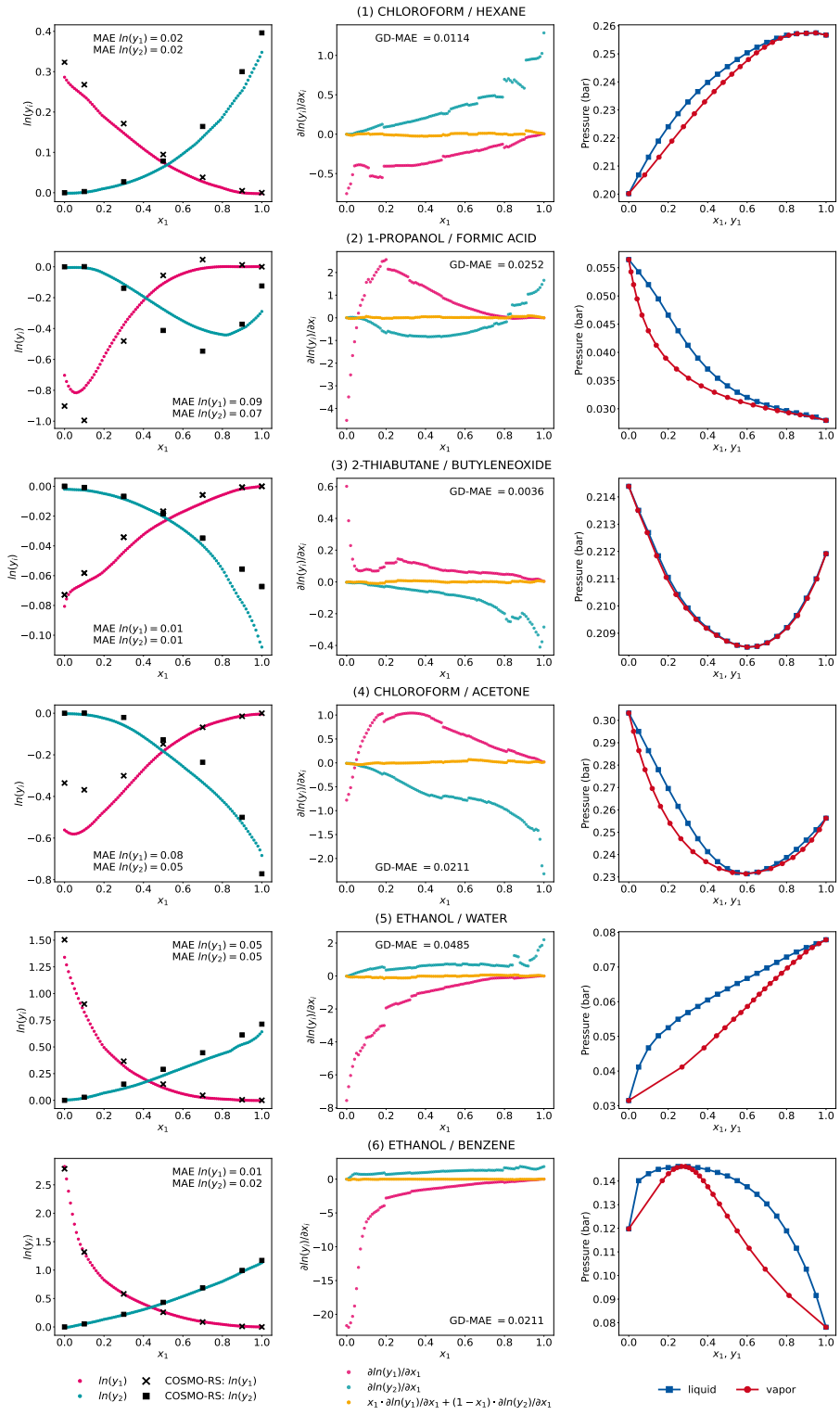

Figure S24: Activity coefficient predictions and their corresponding gradients with respect to the composition and the associated Gibbs-Duhem deviations for exemplary mixtures by the GNN trained with Gibbs-Duhem-informed loss function and following hyperparameters: MLP activation function: softplus, weighting factor $\lambda = 1$, data augmentation: true. Results are from **run 2** of comp-inter split.

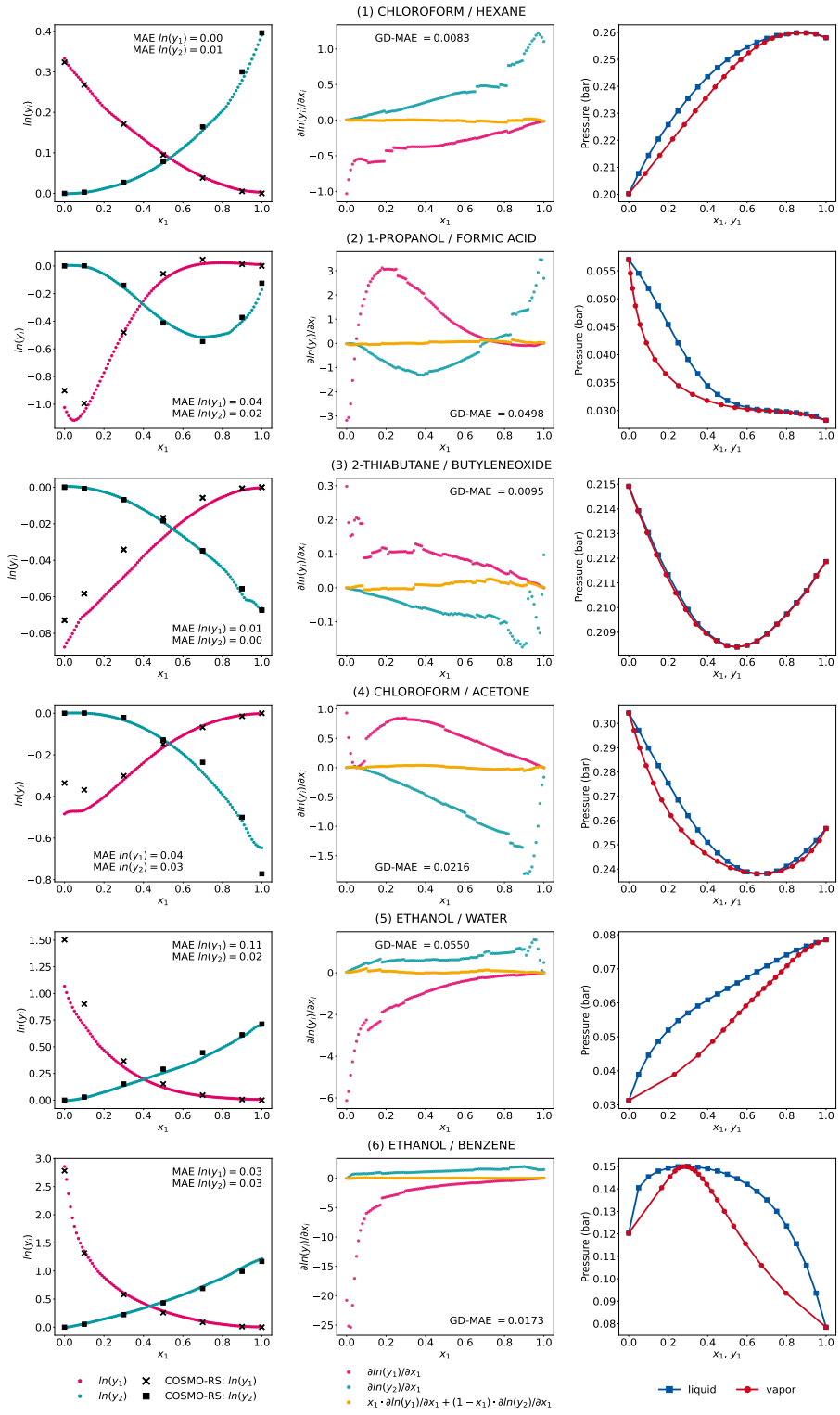

Figure S25: Activity coefficient predictions and their corresponding gradients with respect to the composition and the associated Gibbs-Duhem deviations for exemplary mixtures by the GNN trained with Gibbs-Duhem-informed loss function and following hyperparameters: MLP activation function: softplus, weighting factor $\lambda = 1$, data augmentation: true. Results are from **run 3** of comp-inter split.

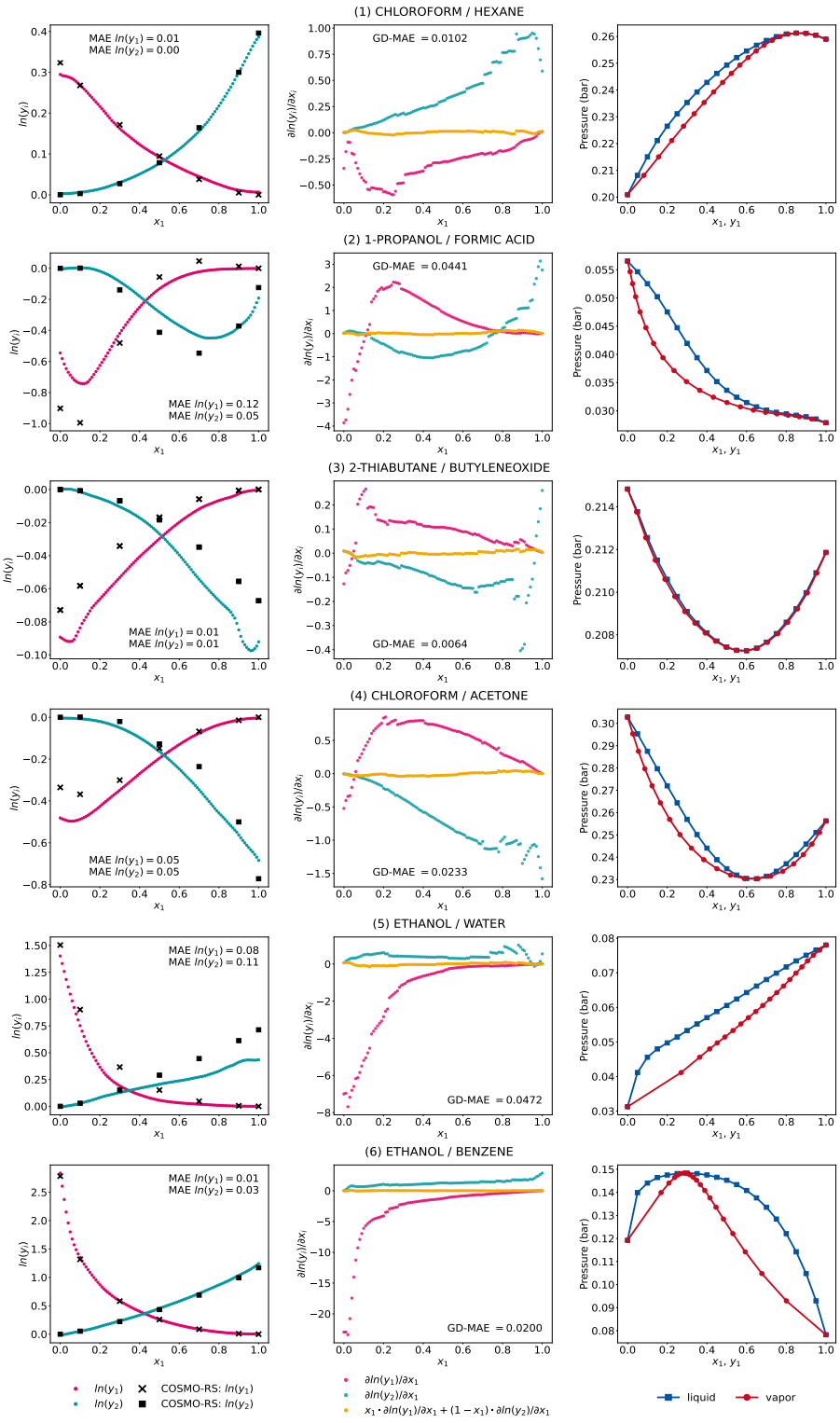

Figure S26: Activity coefficient predictions and their corresponding gradients with respect to the composition and the associated Gibbs-Duhem deviations for exemplary mixtures by the GNN trained with Gibbs-Duhem-informed loss function and following hyperparameters: MLP activation function: softplus, weighting factor $\lambda = 1$, data augmentation: true. Results are from **run 4** of comp-inter split.

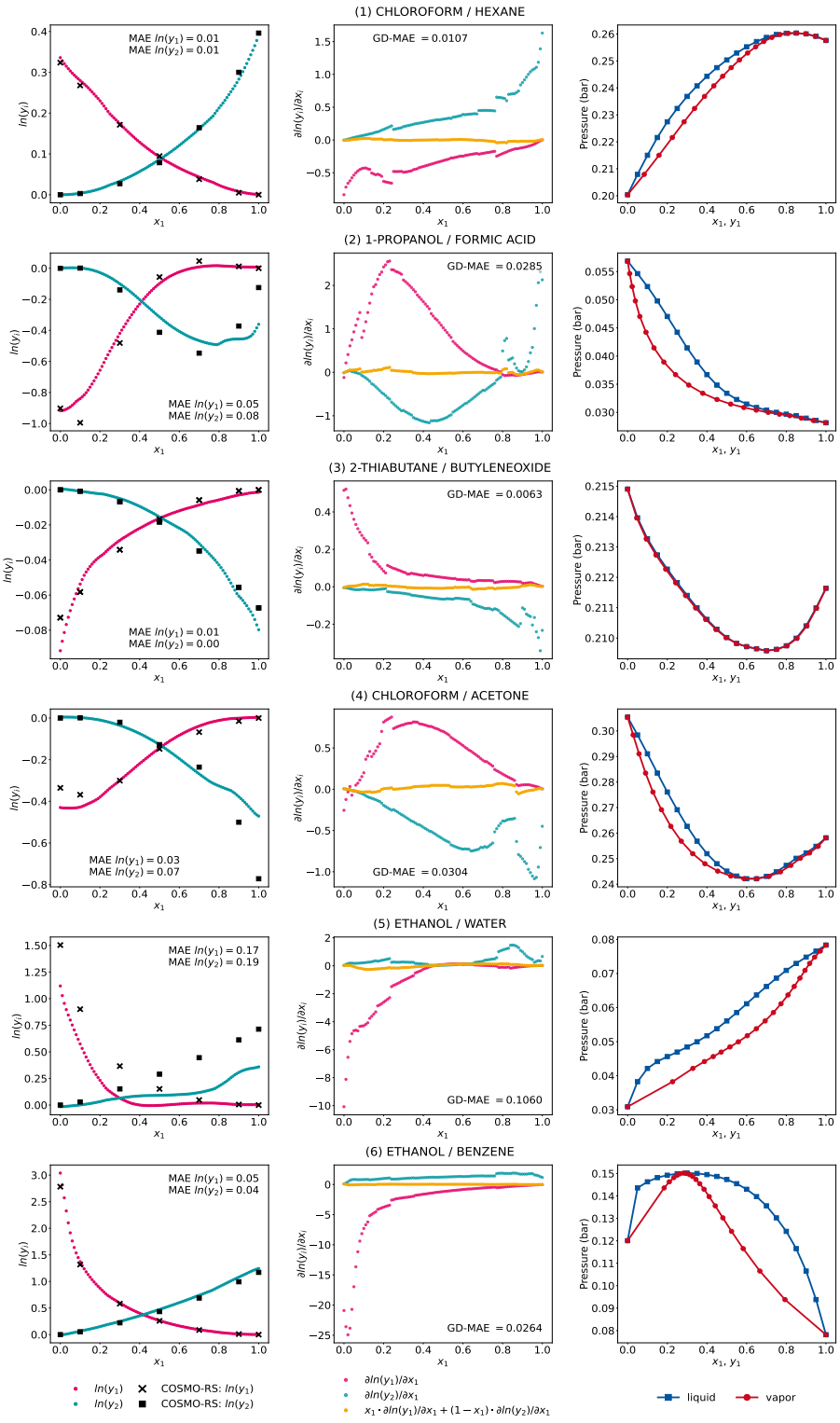

Figure S27: Activity coefficient predictions and their corresponding gradients with respect to the composition and the associated Gibbs-Duhem deviations for exemplary mixtures by the GNN trained with Gibbs-Duhem-informed loss function and following hyperparameters: MLP activation function: softplus, weighting factor $\lambda = 1$, data augmentation: true. Results are from **run 5** of comp-inter split.

69 GDI-MCM:

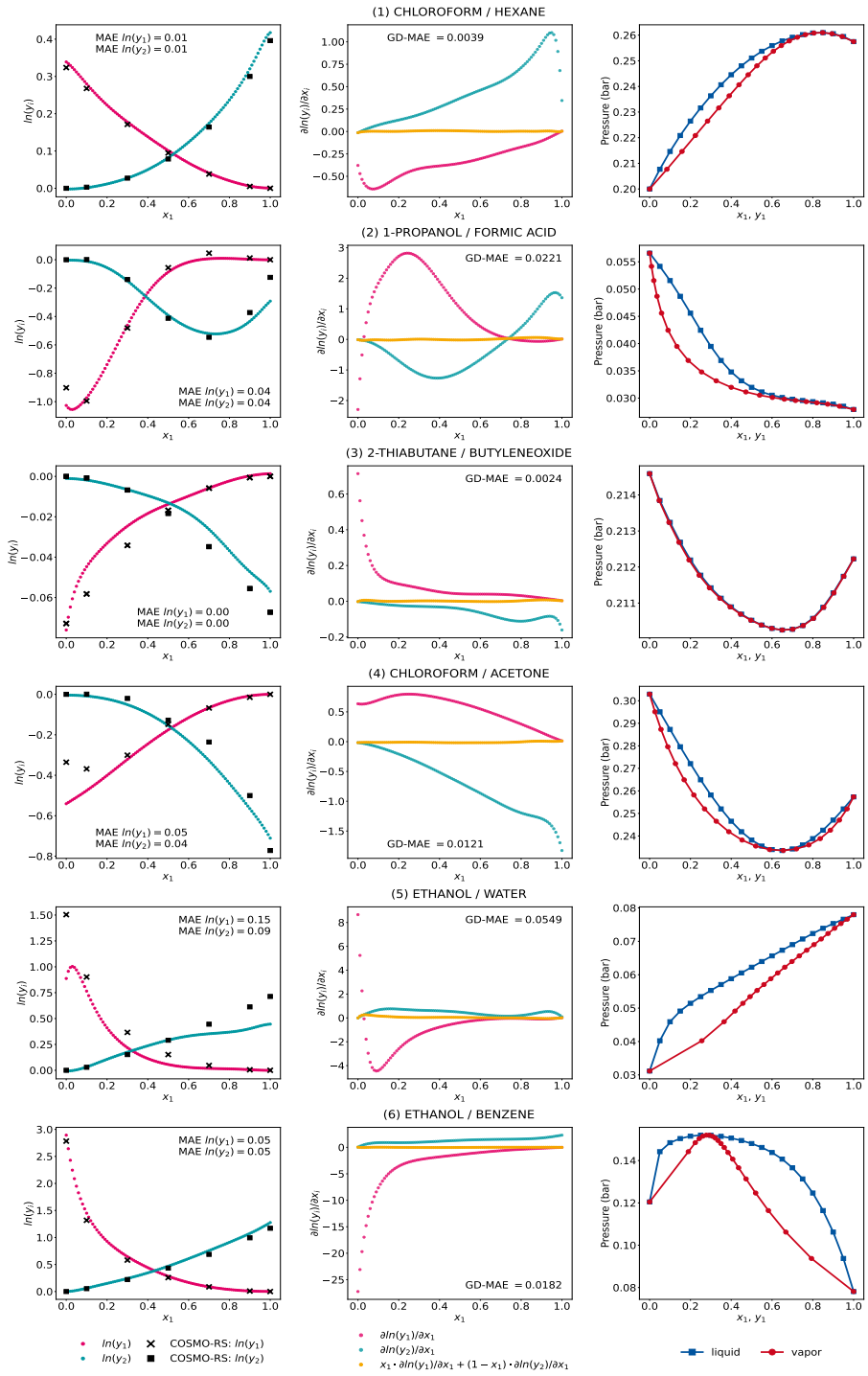

Figure S28: Activity coefficient predictions and their corresponding gradients with respect to the composition and the associated Gibbs-Duhem deviations for exemplary mixtures by MCM trained with Gibbs-Duhem-informed loss function and following hyperparameters: MLP activation function: softplus, weighting factor $\lambda = 1$, data augmentation: true. Results are from **run 1** of comp-inter split.

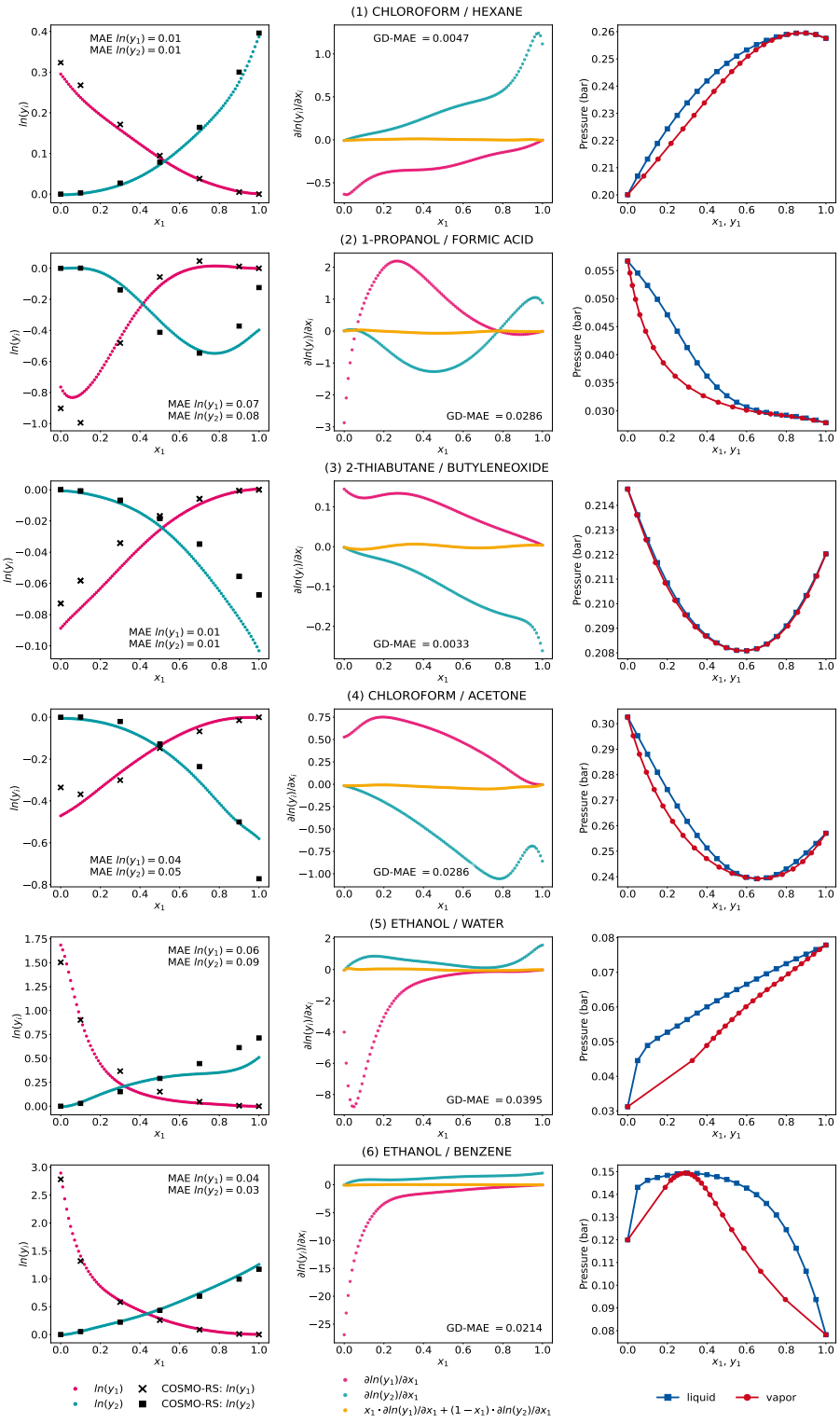

Figure S29: Activity coefficient predictions and their corresponding gradients with respect to the composition and the associated Gibbs-Duhem deviations for exemplary mixtures by MCM trained with Gibbs-Duhem-informed loss function and following hyperparameters: MLP activation function: softplus, weighting factor $\lambda = 1$, data augmentation: true. Results are from **run 2** of comp-inter split.

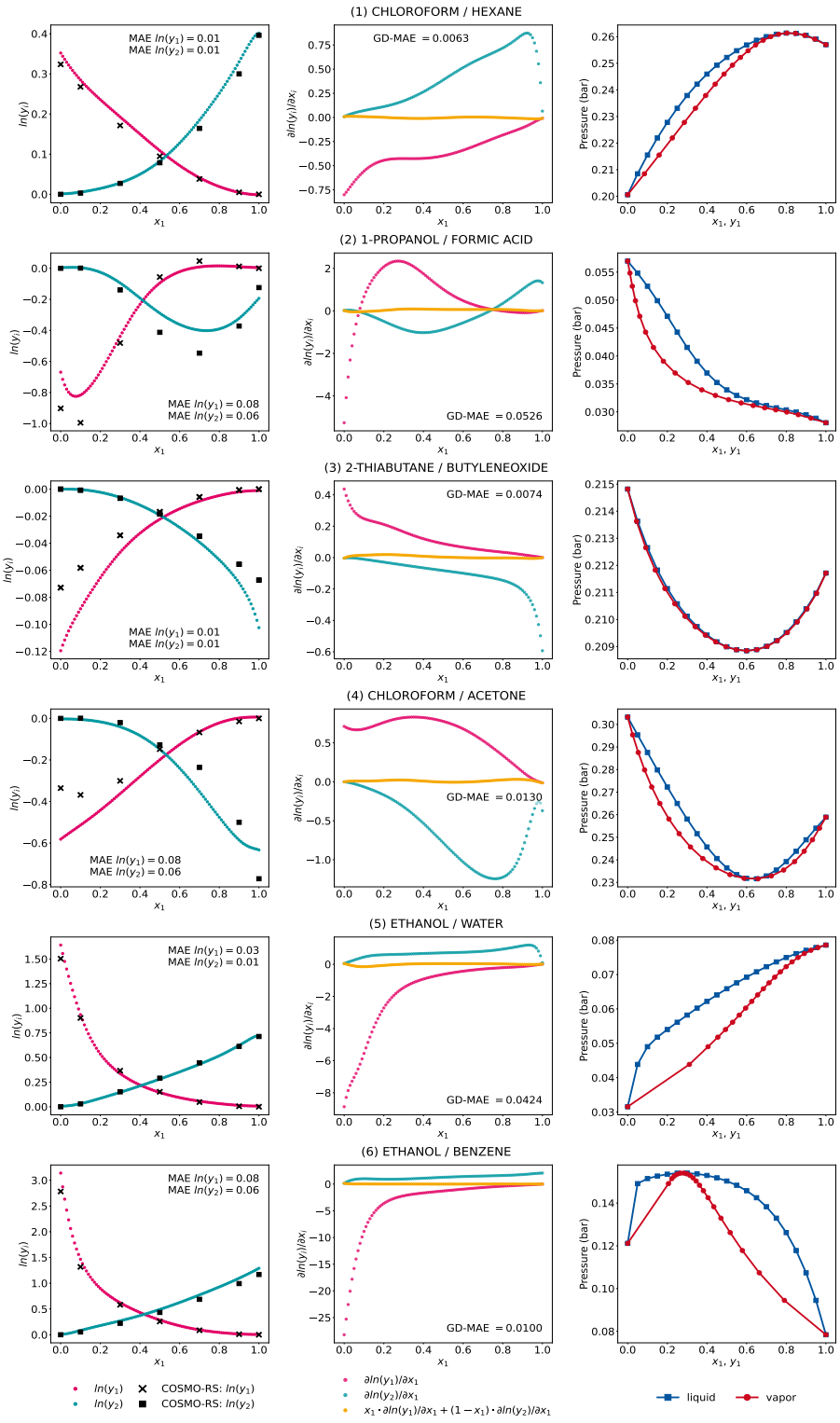

Figure S30: Activity coefficient predictions and their corresponding gradients with respect to the composition and the associated Gibbs-Duhem deviations for exemplary mixtures by MCM trained with Gibbs-Duhem-informed loss function and following hyperparameters: MLP activation function: softplus, weighting factor $\lambda = 1$, data augmentation: true. Results are from **run 3** of comp-inter split.

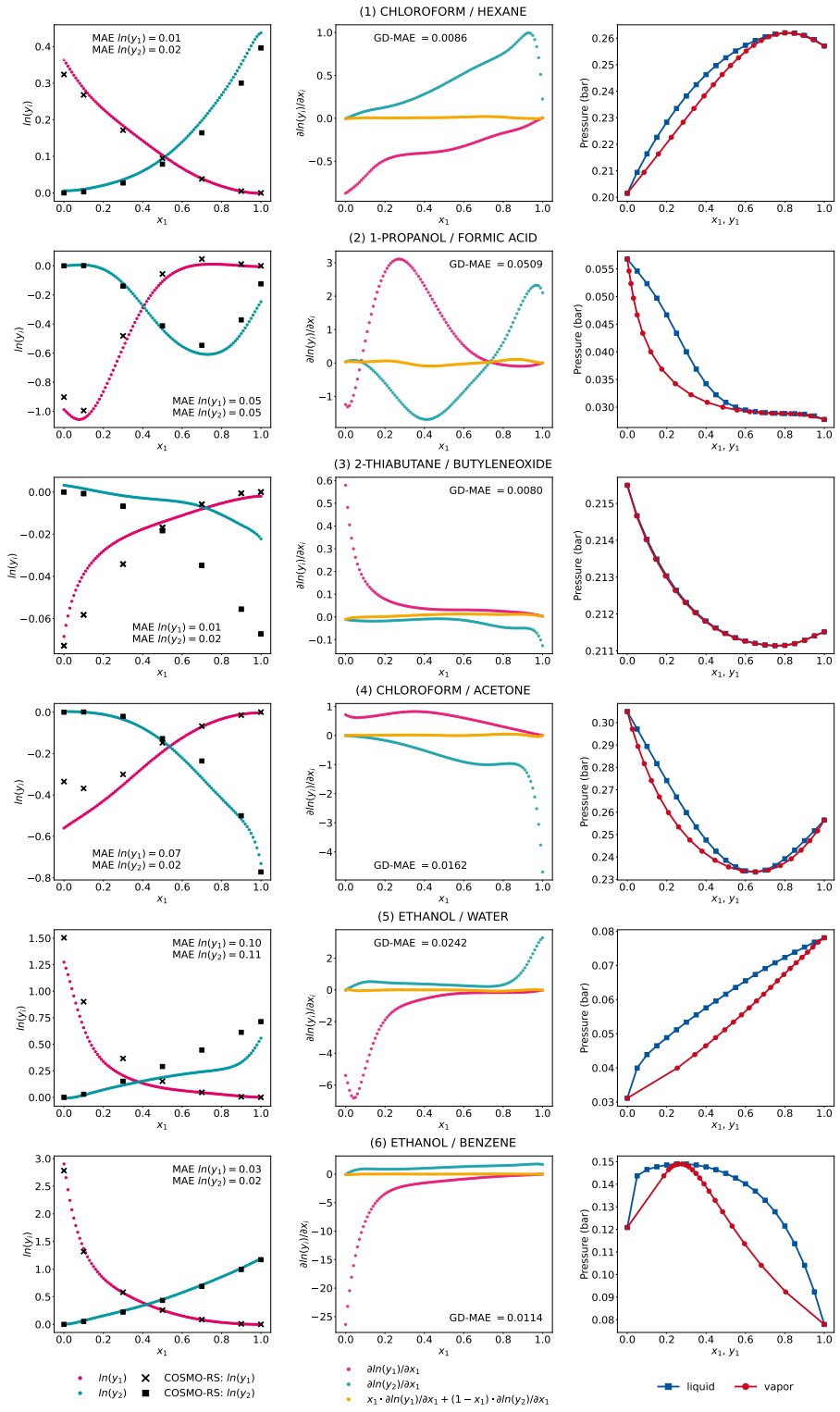

Figure S31: Activity coefficient predictions and their corresponding gradients with respect to the composition and the associated Gibbs-Duhem deviations for exemplary mixtures by MCM trained with Gibbs-Duhem-informed loss function and following hyperparameters: MLP activation function: softplus, weighting factor $\lambda = 1$, data augmentation: true. Results are from **run 4** of comp-inter split.

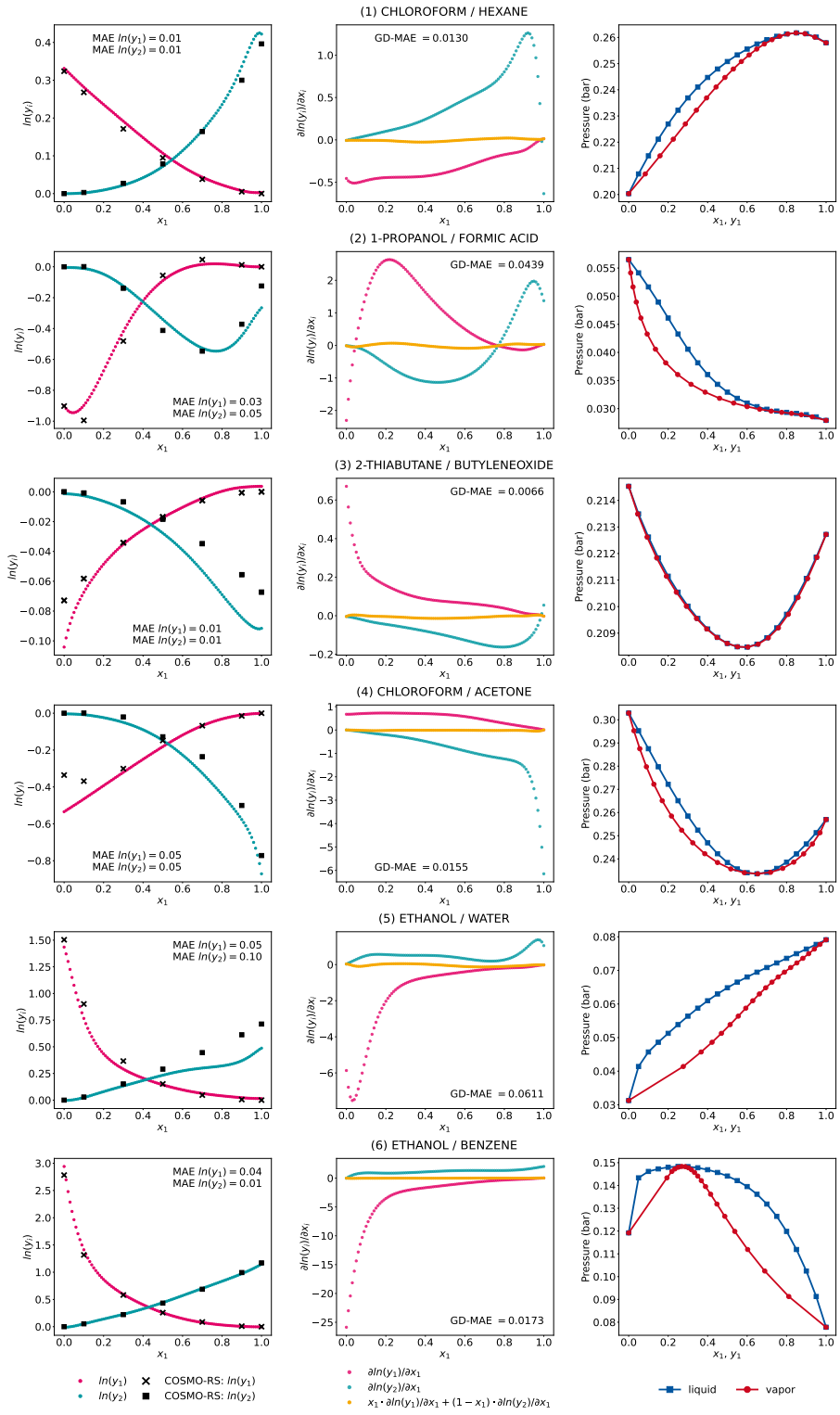

Figure S32: Activity coefficient predictions and their corresponding gradients with respect to the composition and the associated Gibbs-Duhem deviations for exemplary mixtures by MCM trained with Gibbs-Duhem-informed loss function and following hyperparameters: MLP activation function: softplus, weighting factor $\lambda = 1$, data augmentation: true. Results are from **run 5** of comp-inter split.

70 GDI-GNN$_{\text{xMLP}}$:

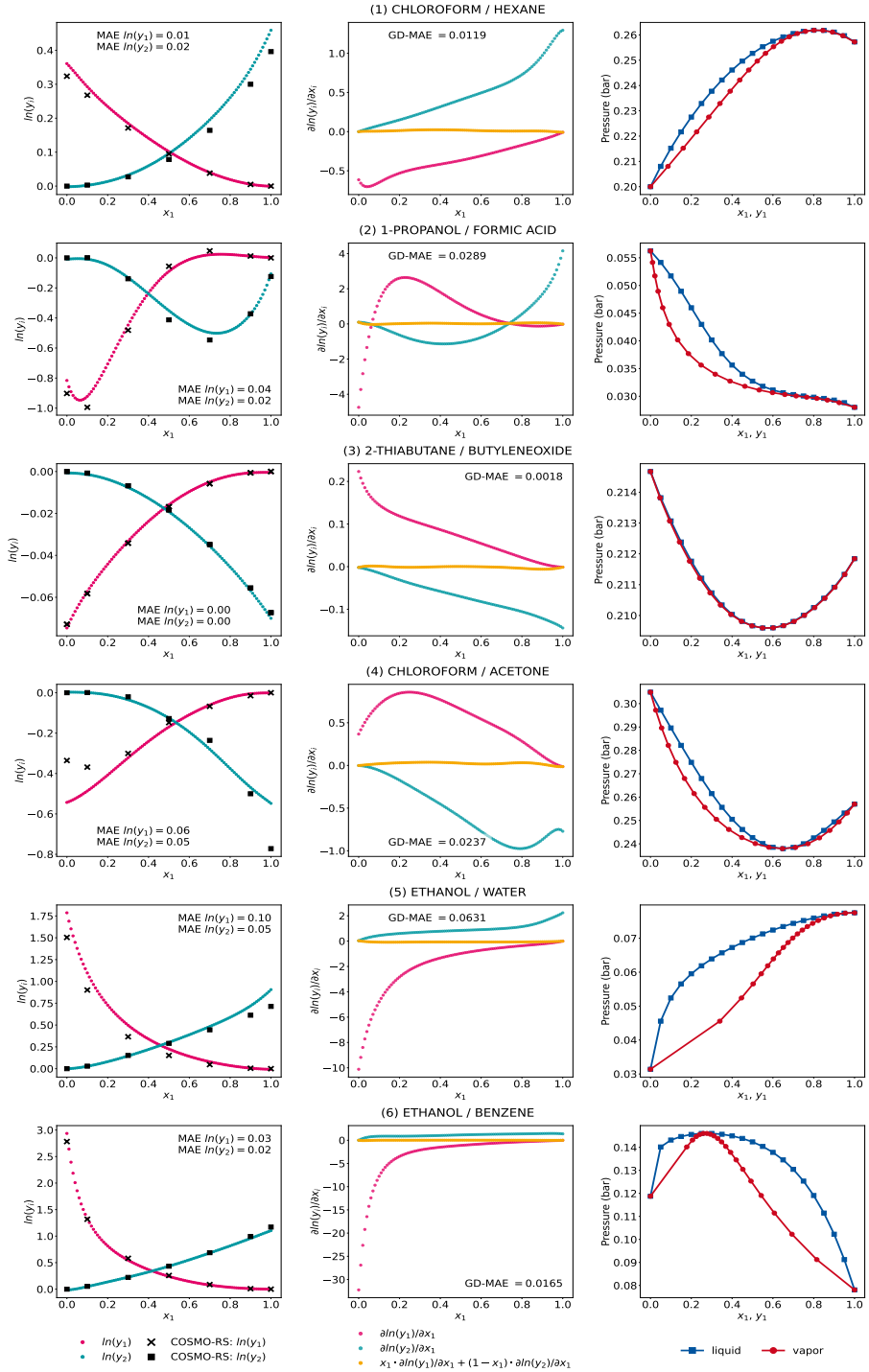

Figure S33: Activity coefficient predictions and their corresponding gradients with respect to the composition and the associated Gibbs-Duhem deviations for exemplary mixtures by the GNN$_{\text{xMLP}}$ trained with Gibbs-Duhem-informed loss function and following hyperparameters: MLP activation function: softplus, weighting factor $\lambda = 1$, data augmentation: true. Results are from **run 1** of comp-inter split.

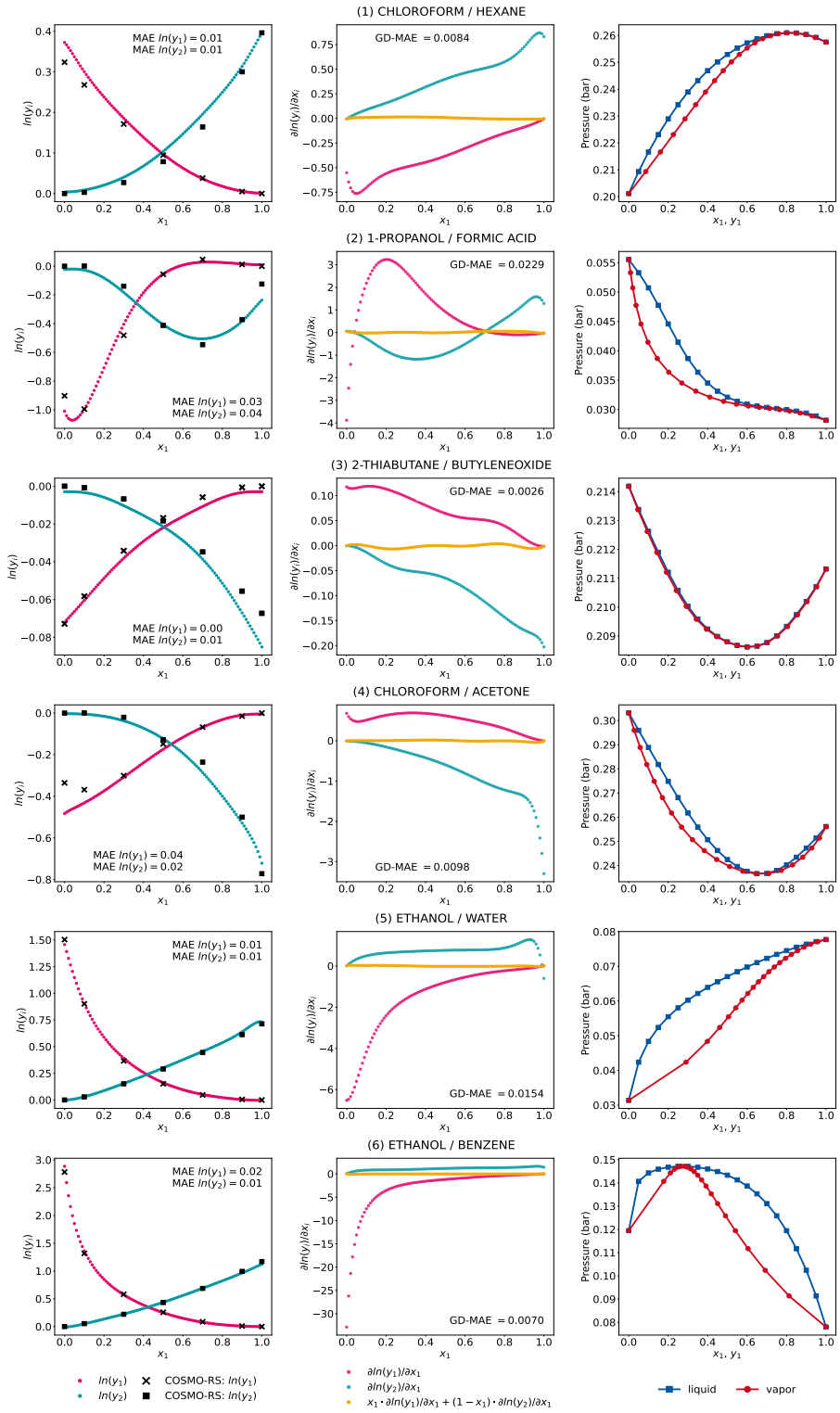

Figure S34: Activity coefficient predictions and their corresponding gradients with respect to the composition and the associated Gibbs-Duhem deviations for exemplary mixtures by the GNN_{xMLP} trained with Gibbs-Duhem-informed loss function and following hyperparameters: MLP activation function: softplus, weighting factor $\lambda = 1$, data augmentation: true. Results are from **run 2** of comp-inter split.

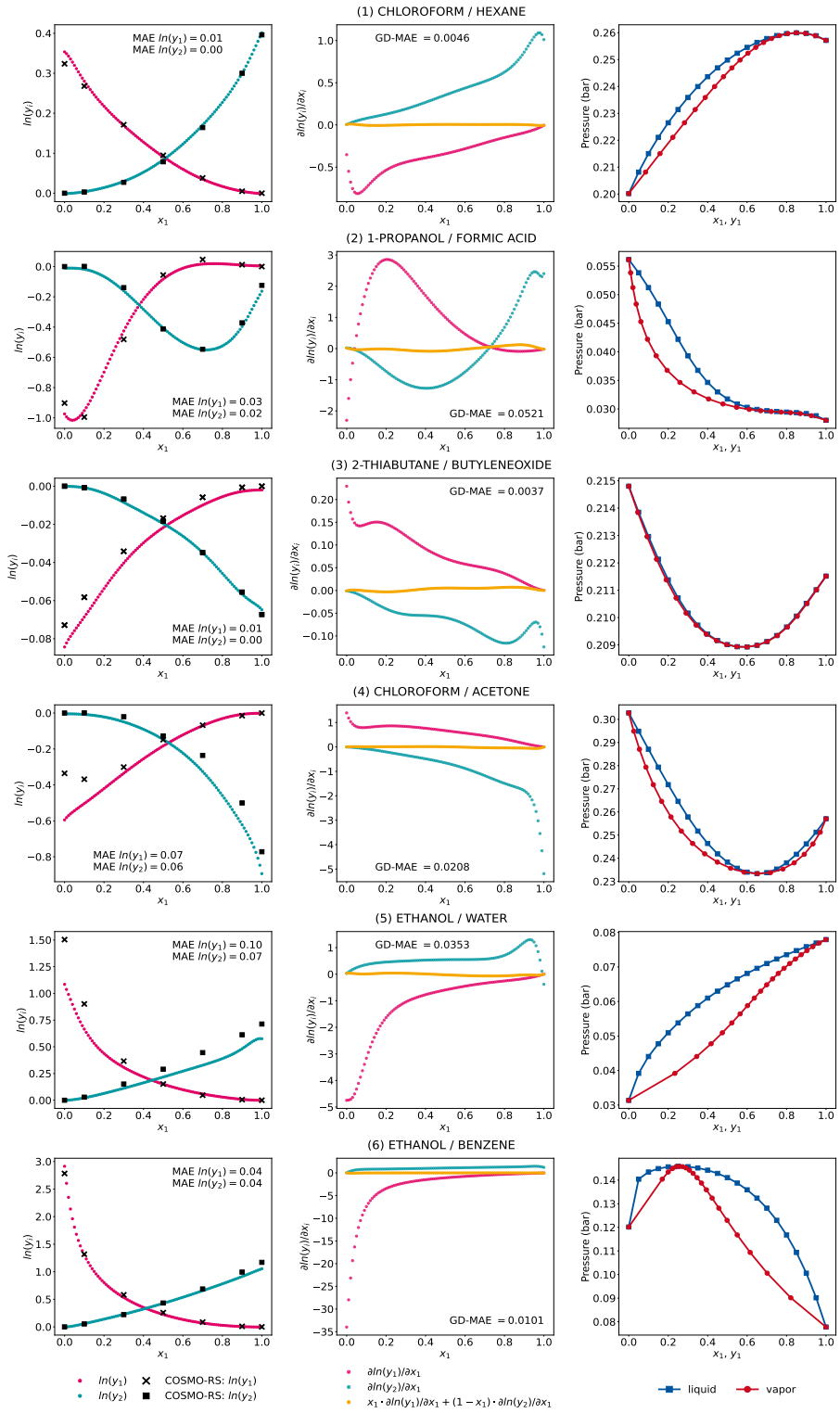

Figure S35: Activity coefficient predictions and their corresponding gradients with respect to the composition and the associated Gibbs-Duhem deviations for exemplary mixtures by the GNN_{xMLP} trained with Gibbs-Duhem-informed loss function and following hyperparameters: MLP activation function: softplus, weighting factor $\lambda = 1$, data augmentation: true. Results are from **run 3** of comp-inter split.

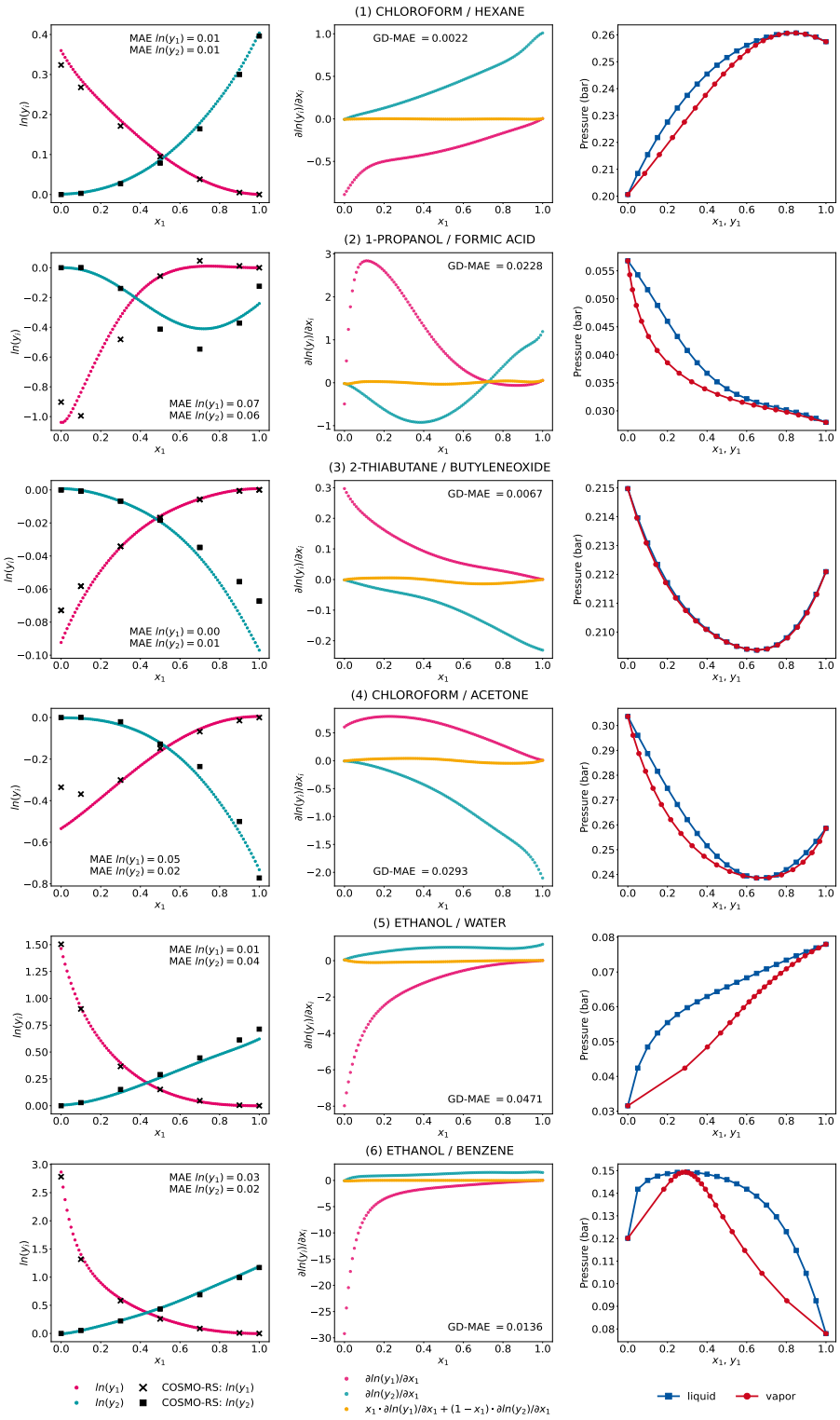

Figure S36: Activity coefficient predictions and their corresponding gradients with respect to the composition and the associated Gibbs-Duhem deviations for exemplary mixtures by the GNN_{xMLP} trained with Gibbs-Duhem-informed loss function and following hyperparameters: MLP activation function: softplus, weighting factor $\lambda = 1$, data augmentation: true. Results are from **run 4** of comp-inter split.

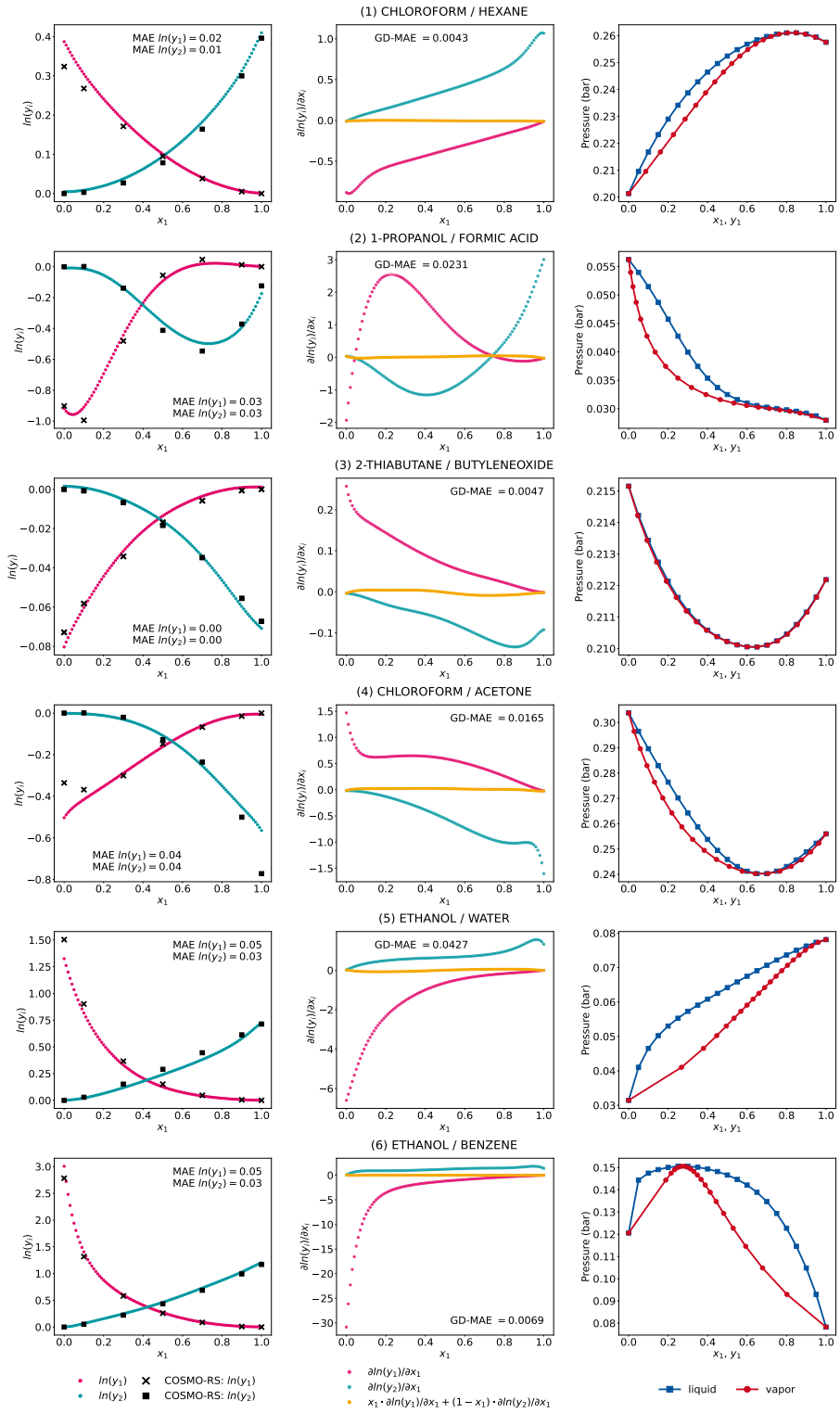

Figure S37: Activity coefficient predictions and their corresponding gradients with respect to the composition and the associated Gibbs-Duhem deviations for exemplary mixtures by the GNN_{xMLP} trained with Gibbs-Duhem-informed loss function and following hyperparameters: MLP activation function: softplus, weighting factor $\lambda = 1$, data augmentation: true. Results are from **run 5** of comp-inter split.

3.3 Gibbs-Duhem-informed training without data augmentation

GDI-GNN:

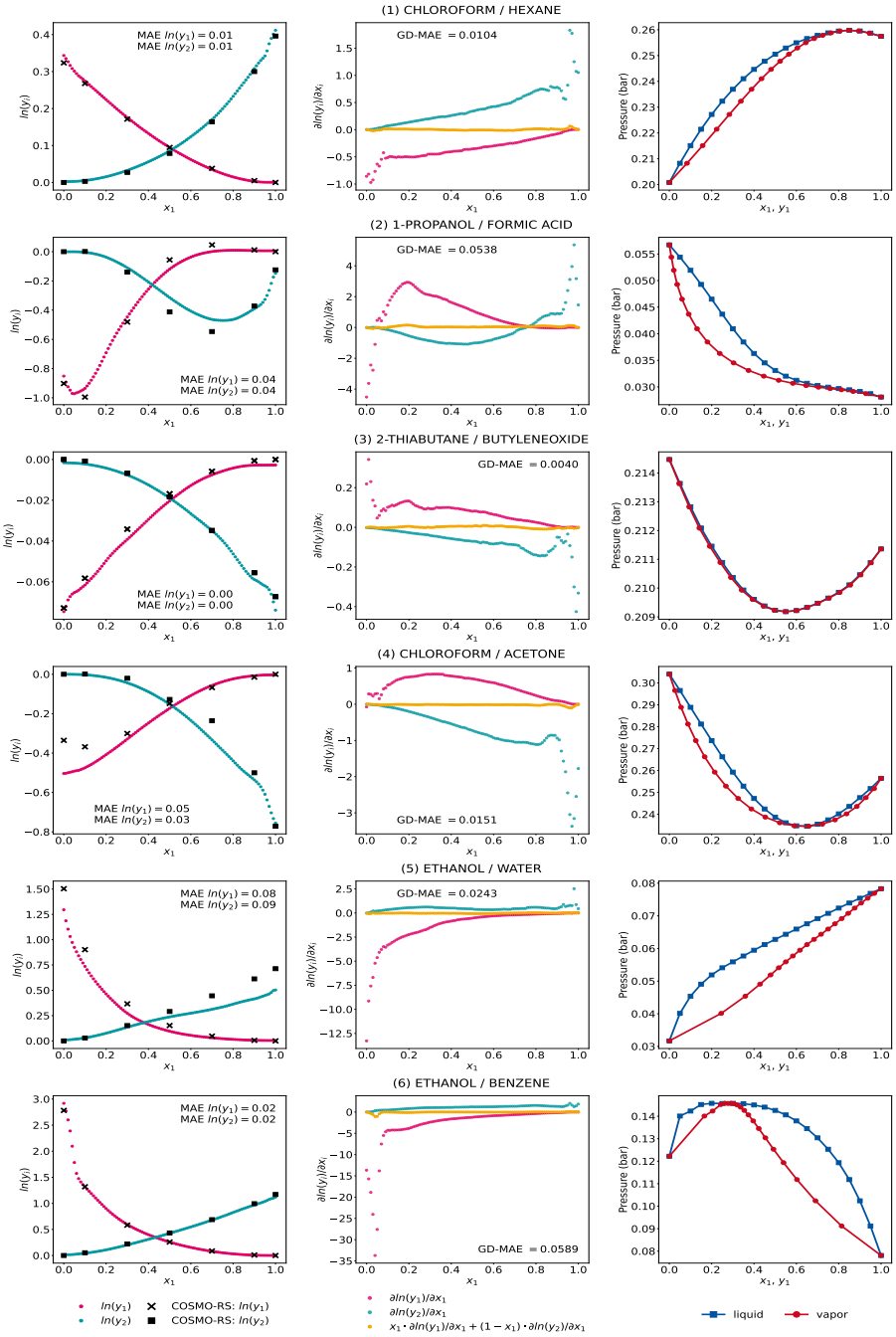

Figure S38: Activity coefficient predictions and their corresponding gradients with respect to the composition and the associated Gibbs-Duhem deviations for exemplary mixtures by the GNN ensemble trained with Gibbs-Duhem-informed loss function and following hyperparameters: MLP activation function: softplus, weighting factor $\lambda = 1$, data augmentation: false. Results are averaged from the five model runs of the comp-inter split

73 GDI-MCM:

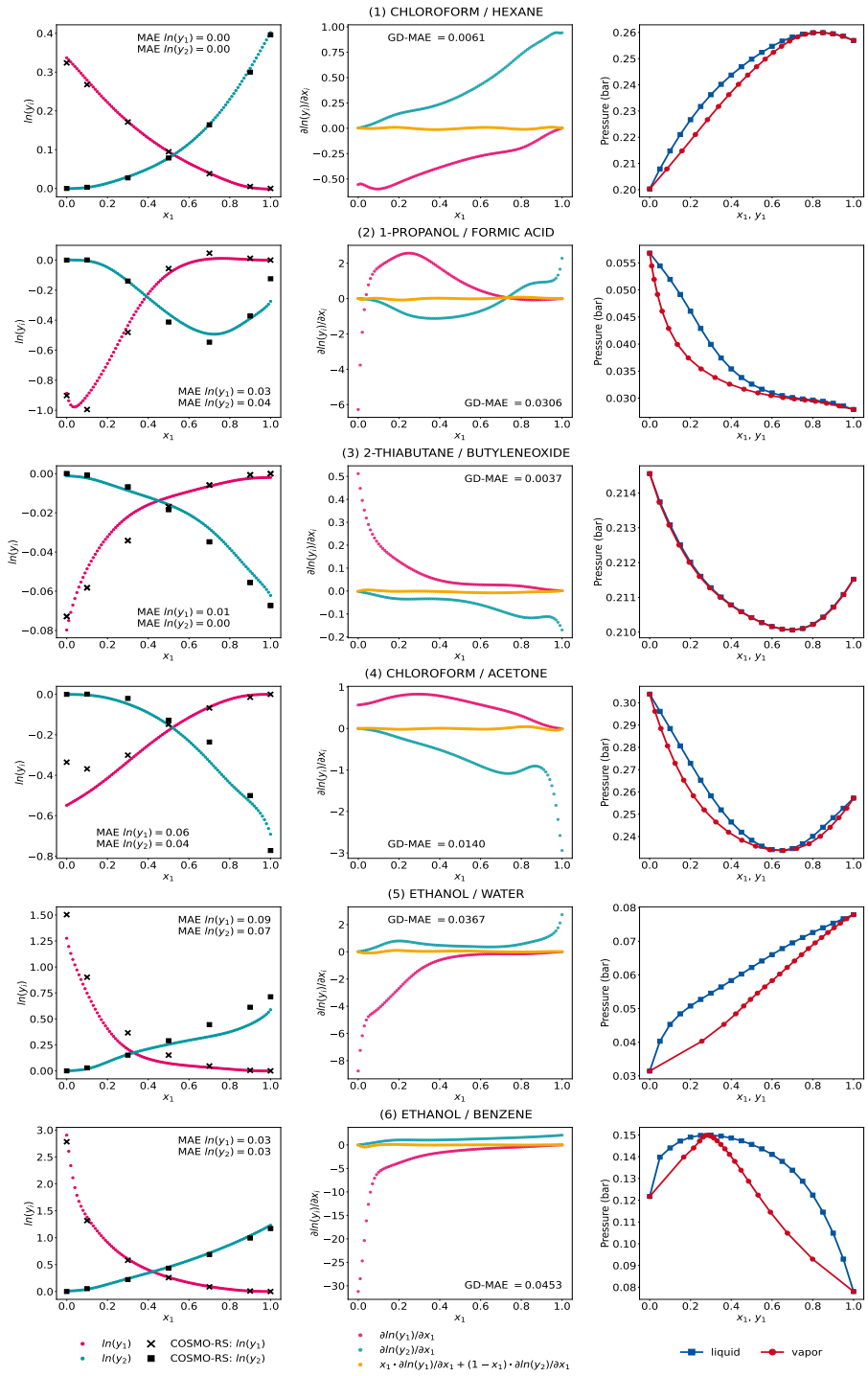

Figure S39: Activity coefficient predictions and their corresponding gradients with respect to the composition and the associated Gibbs-Duhem deviations for exemplary mixtures by the GNN ensemble trained with Gibbs-Duhem-informed loss function and following hyperparameters: MLP activation function: softplus, weighting factor $\lambda = 1$, data augmentation: false. Results are averaged from the five model runs of the comp-inter split.

74 GDI-GNN$_{\text{xMLP}}$:

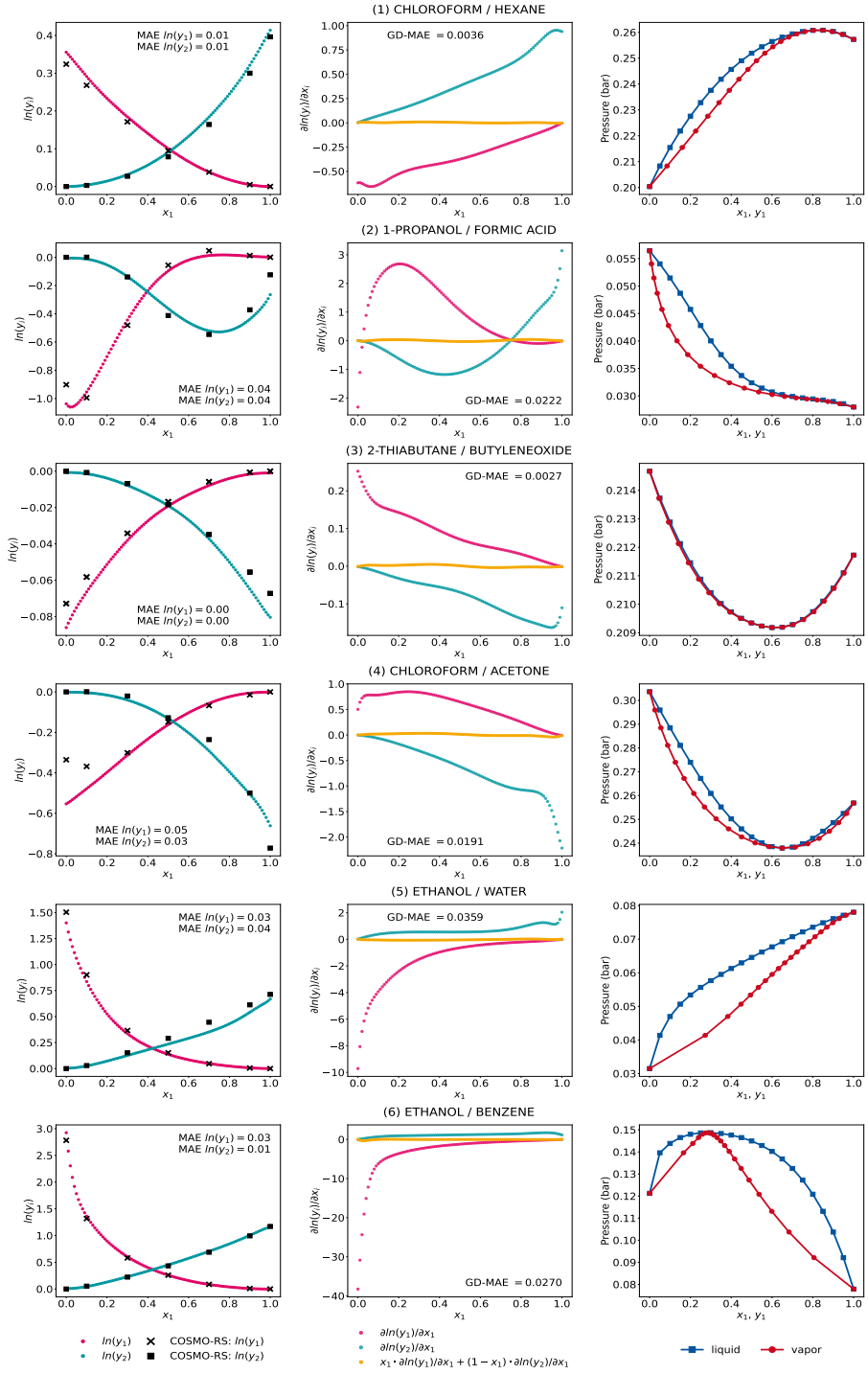

Figure S40: Activity coefficient predictions and their corresponding gradients with respect to the composition and the associated Gibbs-Duhem deviations for exemplary mixtures by the GNN ensemble trained with Gibbs-Duhem-informed loss function and following hyperparameters: MLP activation function: softplus, weighting factor $\lambda = 1$, data augmentation: false. Results are averaged from the five model runs of the comp-inter split.

4 Additional results for Gibbs-Duhem error on external test set

Figure S41 shows the compositions-dependent GD-RMSE for the external test set for the GNN, MCM, and $\mathrm{GNN_{xMLP}}$ with softplus activation for different training setups. The results correspond to the Section "Effect on predictive quality and thermodynamic consistency" in the main text.

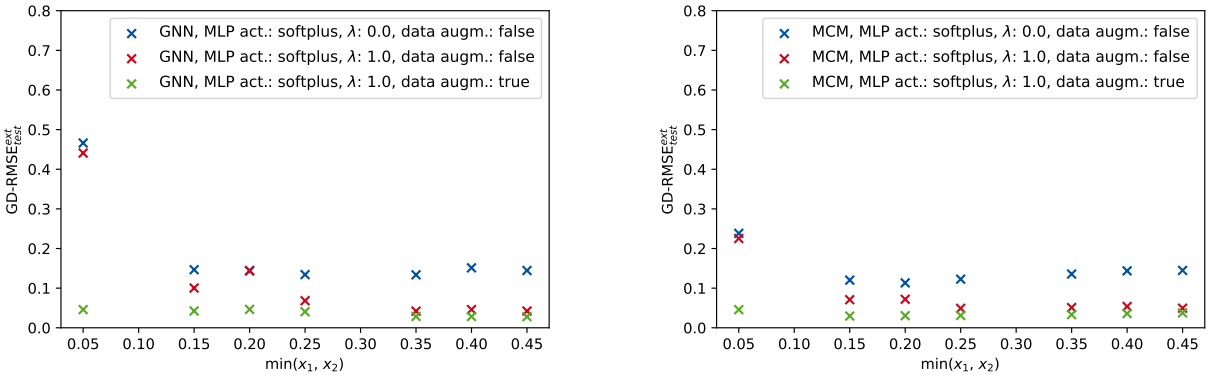

(a) GNN

(b) MCM

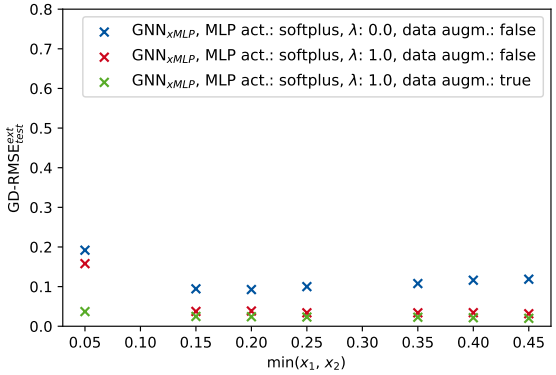

(c) $\mathrm{GNN_{xMLP}}$

Figure S41: Gibbs-Duhem root mean squared error for composition in the external test set for (a) GNN, (b) MCM, (c) $\mathrm{GNN_{xMLP}}$ with with softplus activation, $\lambda = 0$ or 1, and data augmentation: false or true. Models are trained on the comp-inter split.

References

[1] S. Qin, S. Jiang, J. Li, P. Balaprakash, R. C. V. Lehn and V. M. Zavala, *Digital Discovery*, 2023, **2**, 138–151.